Mechanistic three-dimensional model to study centrosome positioning in the interphase cell

Subhendu Som,[*] Saptarshi Chatterjee,[†] and Raja Paul[‡]

Indian Association for the Cultivation of Science, Kolkata - 700032, India

During the interphase in mammalian cells, the position of the centrosome is actively maintained at a small but finite distance away from the nucleus. The perinuclear positioning of the centrosome is crucial for cellular trafficking and progression into mitosis. Although the literature suggests that the contributions of the microtubule-associated forces bring the centrosome to the center of the cell, the position of the centrosome was merely investigated in the absence of the nucleus. Upon performing a coarse-grained simulation study with mathematical analysis, we show that the combined effect of the forces due to the cell cortex and the nucleus facilitate the centrosome positioning. Our study also demonstrates that in the absence of nucleus-based forces, the centrosome collapses on the nucleus due to cortical forces. Depending upon the magnitudes of the cortical forces and the nucleus-based forces, the centrosome appears to stay at various distances away from the nucleus. Such null force regions are found to be stable as well as unstable fixed points. This study uncovers a set of redundant schemes that the cell may adopt to produce the required cortical and nucleus-based forces stabilizing the centrosome at a finite distance away from the nucleus.

I. INTRODUCTION

Proper positioning and orientation of many cellular organelles are crucial for faithful cell division. Centrosome (CS) positioning in the proximity (within 1–$2\,\mu$m) of the nucleus during the interphase is a prime example [1,2]. It is observed that due to the lack of proper CS positioning, several cellular functions, e.g., polarization, migration, and spindle formation, are not successfully completed and as a consequence the cell's survivability is severely compromised [3–5]. The functioning of the key factors responsible for the CS positioning is a fundamental biological question in the context of organelle arrangement in the cell. To explore CS positioning, investigation of the mechanical forces applied on the CS due to the interactions of centrosomal microtubules (MTs) with other cellular objects has been carried out extensively [4,6–9]. MTs are polymeric rods nucleated from the CS uniformly in all directions and have the capability to produce mechanical force (~ 1–100 pN) on the CS via interaction with several cellular components, e.g., cell cortex, cellular membrane, and molecular motors [10,11]. It is observed that MTs pushing against the cell cortex direct the CS toward the cell center while cortical pulling forces drive the CS toward the cell membrane [4,5]. An interplay between these antagonistic forces leads to the proper CS positioning.

Although several computational studies have been performed to investigate CS positioning mediated by the MT driven forces [4,6–9], it is far from clear how the CS is able to maintain a finite distance (i.e., 1–$2\,\mu$m) away from the nucleus during the interphase. The underlying issue with the existing

model systems is that they are built without considering the nucleus. In the absence of the nucleus, MT driven forces can stabilize the CS to the cell center [12–16]. The presence of the nucleus always brings in additional interactions which are challenging to deal with [4,5]; however, it cannot be ignored due to the finite volume of the nucleus and its mechanical interaction with the MTs. The position of the CS is linked with several parameters associated with the MTs, e.g., the growth and shrinkage speed [17], the catastrophe and rescue frequency [5], the flexural rigidity of the MT [4,5], the number of the MTs [5], and the interaction mechanisms of the MTs with the other cellular components [4,5]. In spite of these dependencies, a force balance must be maintained across the parameter regime for a robust mechanism to remain functional [18]. Our goal is to understand the balance of all the forces applied on the CS in the presence of a nucleus that maintains the CS at a perinuclear position.

In order to explore the CS-nucleus interaction, the foremost task is to understand the functions of the force generators when centrosomal MTs interact with the outer nuclear membrane. Clearly, an attractive force between the nucleus and the CS arises when MTs interact via dynein motors lying over the nuclear membrane [1]. This attractive force, however, leads to a collapse of the CS on the nuclear membrane. An adequate repulsive interaction is necessary to keep the CS a finite distance away from the nucleus [19,20]. When a polymerizing MT hits the nuclear membrane and/or buckles in contact with the nuclear membrane, a pushing force is transmitted to the CS via the MT. The interplay between these pushing and pulling forces may play a significant role in positioning the CS.

In the present study we fabricate an agent-based *in silico* model in 3 dimensions (3D) incorporating essential elements of the cell and calculate all the mechanical forces describing CS movement. Unlike a 2-dimensional (2D) model addressed in most of the earlier studies, a 3D model is more appropriate

---
[*]sspss5@iacs.res.in
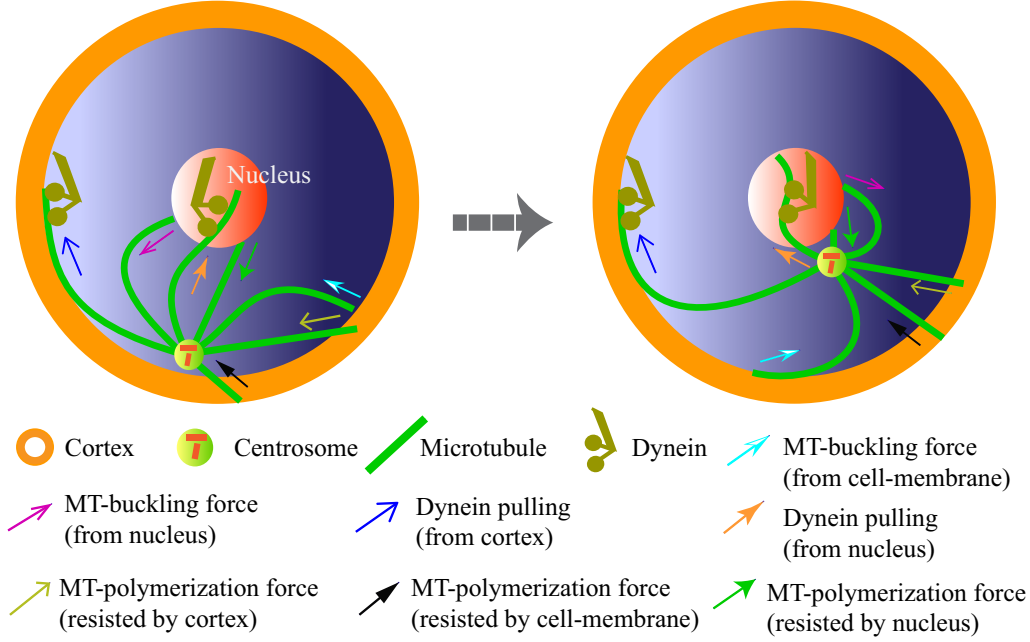[†]sspsc6@iacs.res.in
[‡]ssprp@iacs.res.in

FIG. 1. Schematic representation of various molecular forces acting on the CS from the cortex, the cell membrane, and the nucleus.

for studying mechanical equilibrium of the CS. In order to understand the numerical results, we further develop a mathematical model and observe additional features defining the stability of the CS position. In both these approaches, first we investigate the effect of the individual forces from the cortex and the nuclear membrane and then study their combined effect. While in the presence of the nucleus, the CS remains in the perinuclear region; in the absence of the nucleus, the CS moves to the cell center in agreement with the earlier reports [4,5].

II. COMPUTATIONAL MODEL

We consider the cell, nucleus, and CS as 3D spheres having rigid surfaces and radii r_{cell}, r_{nuc}, and r_{CS}, respectively. MTs are uniformly nucleated from the CS and are assumed to be semiflexible polymers undergoing dynamic instability characterized by the growth velocity v_g, shrinkage velocity v_s, catastrophe frequency f_c, and rescue frequency f_r [4]. When the MTs interact with the cell cortex or cell membrane, pushing and pulling forces are applied on the CS in the following manner (for details see Appendix A and Fig. 1): (1) A pushing force ($\vec{F}_{MT-grow}^{cor}$) is applied on the CS away from the cell cortex when a polymerizing MT penetrates into the cortex [21,22]. (2) An instantaneous pushing force ($\vec{F}_{MT-hit}^{cell-mem}$) is generated on the CS away from the cell membrane, transmitted via the interacting MT tip upon encountering the cell membrane [23]. (3) The CS is pulled toward the cortex [24,25] when negative end directed cortical dynein motors engage with the uncurled MT segment within the cortex. (4) Upon hitting the cell membrane, if the MT keeps on growing, it either buckles in contact with the membrane (determined by a probability $P_{MT-buckle}^{cell-mem}$) or slides along the membrane (determined by a probability $P_{MT-slide}^{cell-mem} = 1.0 - P_{MT-buckle}^{cell-mem}$). Due to the MT buckling transition, a pushing force ($\vec{F}_{MT-buckle}^{cell-mem}$) is generated on the

CS away from the cell membrane [26,27], while the sliding transition generates a pulling force on the CS toward the cortex facilitated by cortical dyneins. The net cortical pulling force ($\vec{F}_{dyn}^{cor}$) includes contributions from both the uncurled and sliding MT segments within the cortex. In a similar manner, MT-nucleus interactions are incorporated in the model as described below (for details see Appendix A and Fig. 1): (1) The CS is pushed away from the nucleus when a polymerizing MT either hits the nuclear membrane [nuclear envelope (NE)] ($\vec{F}_{MT-hit}^{nuc}$) or buckles in contact with the NE ($\vec{F}_{MT-buckle}^{nuc}$) [19,20]. (2) The CS is pulled toward the nucleus ($\vec{F}_{dyn}^{nuc}$) [1] when dynein motors on the nuclear membrane actively engage with the MT and walk toward the negative end of the MT. For simplicity, both the cell cortex and the nucleus are considered as rigid and immobile throughout the simulation. If $\vec{X}_{CS}$ and $\vec{F}_{CS}$ are the instantaneous position of the CS and the resultant force acting on the CS, respectively, according to Stokes law the corresponding equation of motion can be written as

$$\frac{d\vec{x}_{CS}}{dt} = \frac{\vec{F}_{CS}}{\mu_{CS}}, \text{ where}$$

$$\vec{F}_{CS} = \vec{F}_{MT-grow}^{cor} + \vec{F}_{MT-hit}^{cell-mem} + \vec{F}_{dyn}^{cor} + \vec{F}_{MT-buckle}^{cell-mem}$$
$$+ \vec{F}_{MT-hit}^{nuc} + \vec{F}_{MT-buckle}^{nuc} + \vec{F}_{dyn}^{nuc}. \quad (1)$$

Here $\vec{F}_{CS}$ is the net force on the CS (see Appendix A) and μ_{CS} is the effective viscous drag on the CS in cytosol. The resultant force on the CS is calculated by summing over all the force generators mentioned earlier and subsequently the position of the CS is updated over discrete time intervals. As the position of the CS is updated, coordinates of the MT tips are also refreshed by the same instantaneous displacement vector assigned to update the CS position. For instance in a scenario when the CS moves toward the nucleus due to the net force on it resulting in that direction, a microtubule directed toward the opposite direction and previously in contact with

the cell cortex or membrane loses its contact or buckle less. Likewise, a microtubule in contact with the nucleus penetrates more into the nucleus or buckles or slides. A steric force between the CS and cell cortex or nucleus is included to avoid any overlap and for keeping the CS within the cytoplasm.

III. MATHEMATICAL MODEL FOR CENTROSOME POSITIONING: DESCRIPTION OF THE GOVERNING FORCES

Due to symmetry of the problem, we first propose a 1-dimensional (1D) model (for details see Appendix B) in which MTs nucleating from the CS exhibit an exponential length distribution: $N(l) \propto e^{-l/L_{MT}^{av}}$, where L_{MT}^{av} is the average MT length [28]. If the origin is set at the center of the nucleus, x denotes the dynamic position of the centrosome (CS) placed in between the cell membrane and the nucleus. In our model construction when a MT tip encounters the cell membrane, it experiences a pushing force directed opposite to the cell membrane. A MT nucleated from the CS placed at x has to grow a distance $r_{cell} - x$ in order to establish a contact with the cell membrane. The MT elongation up to a distance $r_{cell} - x$ is weighted or regulated by the exponential length distribution taken from a simple phenomenological prescription accounting for modeling the MT dynamic instability [28]. Henceforth, the pushing force generated at the contact of the growing MT tip and the cell membrane is

$$F_{MT-hit}^{cell-mem} = A e^{-(r_{cell}-x)/L_{MT}^{av}}. \quad (2)$$

Similarly, a MT elongating toward the nucleus having the CS placed at x has to grow up to a distance $x - r_{nuc}$ in order to make contact with the NE, and the MT elongation toward the NE is also regulated by the aforementioned exponential distribution. When the concerned MT tip is in contact with the NE, a net push directed away from the NE is experienced at the MT tip interacting with the NE. Henceforth, the pushing force generated at the NE is

$$F_{MT-hit}^{nuc} = A \left(\frac{r_{nuc}}{r_{cell}}\right)^2 e^{-(x-r_{nuc})/L_{MT}^{av}}. \quad (3)$$

Here, A is a constant and proportional to the number of MTs. While interacting with the nucleus, A is scaled by the surface area of the NE relative to the cell membrane in Eq. (3). When a MT penetrates into the cortex, it experiences a pulling from the dyneins anchored at the cortex [11,29]. The net cortical dynein pull on the MTs can be categorized into two parts: (1) dynein pull on the uncurled segment of the MT penetrating into the cortex and (2) dynein pull on the "arc" like MT segment accounting for the MT sliding inside the cortex. Hence, the pulling force toward the cortex is given by

$$F_{dyn}^{cor} = B \lambda_{dyn}^{cor} L_{MT}^{av} \left[\left(e^{l_c/L_{MT}^{av}} - 1\right) e^{-(r_{cell}-2x)/L_{MT}^{av}} \right.$$
$$\left. + e^{-(r_{cell}-x)/L_{MT}^{av}} \right]. \quad (4)$$

Here B is proportional to the number of MTs hitting the cell cortex. λ_{dyn}^{cor} denotes the linear dynein density at the cortex. In the above expression l_c denotes the width of the cortex. The first term in the expression for the net cortical pull [Eq. (4)] corresponds to the contribution from the uncurled MT segment within the cortex whereas the second term accounts

for the contribution from the sliding "arc" like MT segment within the cortex. Similarly when a MT elongates up to the NE and slides along the NE, a net nuclear dynein pull is transduced via the MT to the CS placed at a dynamic location x. Here $x - r_{nuc}$ corresponds to the distance between the CS and NE. Thus a MT directed toward the NE has to grow up to $x - r_{nuc}$ to establish contact with the NE where the MT length is marked by the exponential distribution. The net pulling force arising from the MT-NE interaction toward the nucleus is

$$F_{dyn}^{nuc} = B \left(\frac{r_{nuc}}{r_{cell}}\right)^2 \lambda_{dyn}^{nuc} L_{MT}^{av} e^{-(x-r_{nuc})/L_{MT}^{av}}. \quad (5)$$

Here, λ_{dyn}^{nuc} is the linear dynein density at the NE. Evidently, it turns out that the net dynein pull both at the cortex and NE is proportional to the linear cortical (nuclear) dynein density λ_{dyn}^{cor} (λ_{dyn}^{nuc}), respectively. In Eq. (5), B is scaled by the surface area of the NE relative to the cell membrane. The pushing force generated on the CS due to buckled MTs pivoting at the cell membrane and directed away from the cortex is

$$F_{MT-buckle}^{cell-mem} = \frac{D}{(r_{cell} - x)^2} e^{-(r_{cell}-x)/L_{MT}^{av}}. \quad (6)$$

Here D is proportional to the number of MTs undergoing buckling at the cortex. We have considered semiflexible MTs undergoing Euler buckling in the first mode [5]. In Eq. (6), the factor $r_{cell} - x$ corresponds to the distance between the CS (placed at x) and the pivot point at the cell membrane where the concerned MT tip undergoing buckling transition is anchored. Similarly, the pushing force directed away from the nucleus due to the buckling of the MTs pivoting at the NE is

$$F_{MT-buckle}^{nuc} = \frac{D'}{(x - r_{nuc})^2} e^{-(x-r_{nuc})/L_{MT}^{av}}. \quad (7)$$

In Eq. (7), $x - r_{nuc}$ is the shortest distance between the CS (placed at x) and NE. Clearly, a MT directed toward the NE has to grow up to a length $x - r_{nuc}$ to establish contact with the NE and undergo the buckling transition via pivoting at an anchorage on the NE. Here, D' being proportional to the number of MTs undergoing buckling at the NE can be approximated as $D(\frac{r_{nuc}}{r_{cell}})^2$ since the number of MTs falling onto the NE is proportional to the surface area of the nucleus. Following a similar approach, we have also developed a mathematical model for the CS positioning in 2D (see Appendix C).

IV. SIMULATION

We mimic the dynamic instability of the MTs using four intrinsic parameters (v_g, f_c, v_s, and f_r) of the polymer. The simulation was carried out with literature-based values for most of the parameters and the remaining parameters (probability of MT buckling or sliding at cell membrane or nuclear membrane and dynein density on the NE) chosen wisely (Table I). More specifically, we explored the range of parameters where we observed characteristic changes in the stability of the centrosomal position within the cell. For instance, the probabilities for the buckling or sliding transitions, dynein densities at the cortex and NE, and average MT length have been scanned across an extended regime and the sensitivity

TABLE I. Model parameters.

Abbreviations	Meaning	Values used	Reference
r_{cell}	Cell radius	$10\,\mu\text{m}$	[5]
r_{nuc}	Nucleus radius	$3\,\mu\text{m}$	[36]
r_{CS}	Centrosome radius	$0.5\,\mu\text{m}$	[5]
v_g/v_s	Growth/shrinkage speed of the MTs	$7.5/16\,\mu\text{m min}^{-1}$	[4]
f_c/f_r	Catastrophe/rescue rate of the MTs	$2/4\,\text{min}^{-1}$	[4]
f_c^{stall}	Stall catastrophe rate of the MTs	$2.4\,\text{min}^{-1}$	[5]
f_{stall}	Stall force of the MTs	$1.7\,\text{pN}$	[23]
k_{cor}	Spring constant of the cortex	$4\,\text{pN}\,\mu\text{m}^{-1}$	[23]
L_p	Persistence length of the MT	$5200\,\mu\text{m}$	[5,35]
$\lambda_{\text{dyn}}^{\text{cor}}$	Cortical dynein density	$0.03\,\mu\text{m}^{-1}$ (WT)	[4]
$\lambda_{\text{dyn}}^{\text{nuc}}$	Nuclear dynein density	$0.03\,\mu\text{m}^{-1}$ (WT)	This study
L_{MT}^{av}	Average MT length	$60\,\mu\text{m}$ (WT)	[4]
f_{dyn}^s	Force produced by a single dynein	$1\,\text{pN}$	[4]
μ_{CS}	Viscous drag of the CS	$\sim2000\,\text{pN s}\,\mu\text{m}^{-1}$	[5]
$P_{\text{MT-buckle}}^{\text{nuc}}/ P_{\text{MT-buckle}}^{\text{cell-mem}}$	MT buckling probability at nucleus/ cell membrane	0.5	This study
$P_{\text{MT-slide}}^{\text{nuc}}/ P_{\text{MT-slide}}^{\text{cell-mem}}$	MT sliding probability at nucleus/ cell membrane	0.5	This study

analyses are performed on these parameters. The nucleus is assumed to be static at the cell center and Eq. (1) is used to update the coordinates of the CS. Choosing the time steps 0.01 s (typically much smaller than the time needed to grow a MT about the size of the cell), we simulate the system for ~1 h which is sufficiently large for obtaining a steady state configuration.

V. RESULTS

In order to comprehend the effects of the cortical and the nucleus-based forces on the CS positioning, we explore the distributions of these forces across the permissible range of the CS position and evaluate centrosomal trajectories under these forces. The forces directed outward from the nucleus are chosen positive, while inward directed forces are denoted by a negative sign. Consequences of individual and combined forces are summarized below.

A. Interplay among a myriad of cortical forces fails to render the proper perinuclear positioning of the centrosome

The net pushing force on the CS from the cortex, $F_{\text{push(net)}}^{\text{cor}}$, essentially comes from the MT polymerization force ($F_{\text{MT-grow}}^{\text{cor}}$), the MT buckling force ($F_{\text{MT-buckle}}^{\text{cell-mem}}$), and the MT impact force ($F_{\text{MT-hit}}^{\text{cell-mem}}$) (see Appendix A). Our study reveals that the CS lands on the NE if this pushing force from the cortex is the only driving force [see Fig. 2(a)]. In the absence of cortical pushing, forces pulling the CS toward the cortex (cortical pulling force $F_{\text{pull}}^{\text{cor}}$) bring the CS to the cell membrane [Fig. 2(b)]. $F_{\text{pull}}^{\text{cor}}$ is the net force due to dynein motors, acting on the MTs (Appendix A). To elucidate these results further [Figs. 2(a) and 2(b)], we investigate the distributions of $F_{\text{push(net)}}^{\text{cor}}$ and $F_{\text{pull}}^{\text{cor}}$ across the whole permissible range of CS position, i.e., throughout the region between the NE and the cell membrane [Fig. 2(c)]. Notice that the cortical pushing force (asterisk) is nonzero on the CS through the entire range of the CS position and is directed toward the NE (negative force is directed toward the NE). However, the magnitude of

$F_{\text{push(net)}}^{\text{cor}}$ rapidly falls off with the decrease of the CS-nucleus distance (center to center). As observed, lengths of the MTs (L_{MT}) buckled from the cell membrane increase when the CS moves away from the cell membrane; therefore, the Euler buckling force, $F_{\text{MT-buckle}}^{\text{cell-mem}} \propto L_{\text{MT}}^{-2}$, a major component of $F_{\text{push(net)}}^{\text{cor}}$, weakens as a function of the CS-nucleus distance. The cortical pulling force toward the cell membrane appears to remain finite and vary less compared to the cortical pushing force throughout the range of the CS position. The CS always moves toward the cell membrane when $F_{\text{pull}}^{\text{cor}}$ independently determines the CS position.

To examine the resultant effect of the cortical push ($F_{\text{push(net)}}^{\text{cor}}$) and pull ($F_{\text{pull}}^{\text{cor}}$) on the CS positioning, these forces are applied simultaneously on the CS and the centrosomal trajectory is recorded [Fig. 2(d)]. Due to the effect of the resultant cortical force ($F_{\text{total}}^{\text{cor}}$), the CS falls on the NE in a similar manner to that under $F_{\text{push(net)}}^{\text{cor}}$ [Fig. 2(a)]. Thus we plot $F_{\text{total}}^{\text{cor}}$ as a function of CS-nucleus distance in Fig. 2(e) and compare with $F_{\text{push(net)}}^{\text{cor}}$ shown in Fig. 2(c). Interestingly, the characteristics of these two forces appear to be very similar, indicating $F_{\text{push(net)}}^{\text{cor}}$ completely dominating over $F_{\text{pull}}^{\text{cor}}$ and guiding the CS movement according to $F_{\text{push(net)}}^{\text{cor}}$. To test the effect of the resultant cortical force on the CS positioning when the nucleus is off-centered (see Appendix D for details), we investigate $F_{\text{total}}^{\text{cor}}$ as a function of CS-nucleus distance. We find that irrespective of the nuclear position, $F_{\text{total}}^{\text{cor}}$ is always directed toward the NE. These results suggest that for any arbitrary position of the CS and the nucleus, the resultant cortical force on the CS always drives it to fall on the NE.

Since the cortical dynein density on the MT is taken to be small ($0.03\,\mu\text{m}^{-1}$), it is expected that the pulling force toward the cortex is largely suppressed by the strong pushing force away from the cortex. Thus, we further investigate [Fig. 2(f)] whether an enhanced cortical dynein density ($\lambda_{\text{dyn}}^{\text{cor}}$) can bring any significant change in the CS position. We find that the cortical pulling force can completely neutralize the cortical pushing force (the black line) only when CS is adjacent to the NE (i.e., close to $3.5\,\mu\text{m}$ line) and the cortical dynein density is very high (i.e., $\sim4\,\mu\text{m}^{-1} < \lambda_{\text{dyn}}^{\text{cor}} \leqslant 10\,\mu\text{m}^{-1}$). It
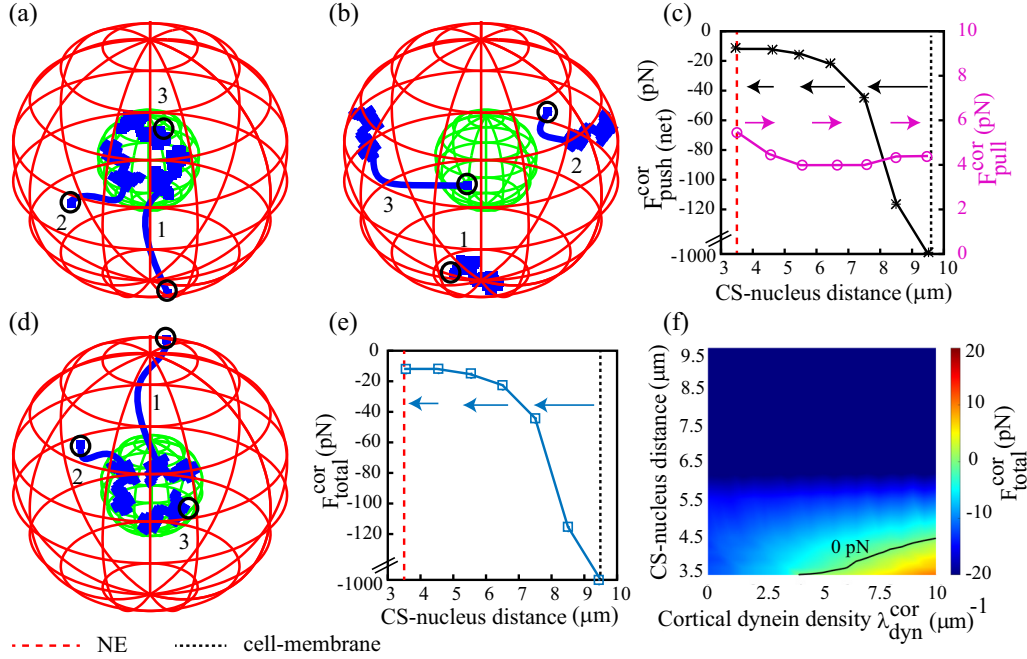
FIG. 2. Effects of the cortical forces on the CS positioning. In (a) and (b), cell, nucleus, and CS trajectories are represented by the outer (red) sphere, the inner (green) sphere, and the (blue) lines, respectively. Open (black) circle in each CS trajectory marks the initial position of the CS where (1) CS initially lies on the cell membrane, (2) CS initially lies in between the cell membrane and the nucleus, and (3) CS initially lies on the nucleus. Irrespective of the initial position of the CS, (a) it finally arrives at the NE subjected to the net cortical pushing force, (b) it finally lands on the cell membrane subjected to the cortical pulling force. (c) The net cortical pushing force, $F_{\text{push(net)}}^{\text{cor}}$ (asterisk), falls from a large value (~-1000 pN) to a small value (~-10 pN) as the distance between CS and nucleus decreases from the maximum (9.5 μm) to minimum (3.5 μm) and is directed (the leftward vector arrows) toward the NE. The cortical pulling force, $F_{\text{pull}}^{\text{cor}}$ (open circles), persists at a small value (~4–6 pN) on the CS throughout the entire range of CS position and is directed (the rightward vector arrows) away from the NE. (d) CS is finally found on the NE when all the cortical forces simultaneously act on the CS. (e) The combined cortical force on CS, $F_{\text{total}}^{\text{cor}}$, is directed toward the NE (the leftward vector arrows) and the characteristic of this force is very similar to the net cortical pushing force (c). (f) The black line in the heat map represents the locus of the zero force region (stable fixed point) of the CS. CS does not collapse on the NE (3.5 μm line) when the cortical dynein density becomes very high ($\lambda_{\text{dyn}}^{\text{cor}} \gtrsim 4 \ \mu\text{m}^{-1}$).

turns out that a properly positioned CS (~1–2 μm away from the nucleus) can be achieved when $\lambda_{\text{dyn}}^{\text{cor}}$ is extremely large ($\sim10 \ \mu\text{m}^{-1}$), which is likely to be irrelevant for any practical purposes [4].

B. Centrosome is pushed to the cell membrane by the nucleus mediated forces

To explore the effects of the nucleus mediated forces on the CS position, we incorporate feasible MT-nucleus interactions in our study (see Appendix A). The net pushing force imparted on the CS ($F_{\text{push(net)}}^{\text{nuc}}$) due to the nucleus is composed of the Euler buckling force ($F_{\text{MT}-\text{buckle}}^{\text{nuc}}$) and the force applied by the polymerizing MTs $F_{\text{MT}-\text{hit}}^{\text{nuc}}$ (Appendix A). Our study reveals that the CS is strongly pushed toward the cell membrane when the nuclear pushing force alone drives the CS [see Fig. 3(a)]. A pulling force $F_{\text{pull}}^{\text{nuc}} = F_{\text{dyn}}^{\text{nuc}}$ is applied on the CS by the nucleus (nuclear pulling force) when the MTs engage with the dynein motors lying over the NE (Appendix A). In the absence of any other forces, the nuclear pulling force brings the CS onto the NE [Fig. 3(b)]. In order to gain further insight on how these forces behave spatially, we investigate the distributions of $F_{\text{push(net)}}^{\text{nuc}}$ and $F_{\text{pull}}^{\text{nuc}}$ across the whole permissible range of CS position [Fig. 3(c)]. Notice that $F_{\text{push(net)}}^{\text{nuc}}$ is very high and directed away from the nucleus (positive force) when the CS

is close to the NE; this force falls off exponentially with the increase of the CS-nucleus distance. Essentially, $F_{\text{push(net)}}^{\text{nuc}}$ follows the behavior of the dominant force contributor, i.e., the Euler buckling force of the MT $F_{\text{MT}-\text{buckle}}^{\text{nuc}} \propto L_{\text{MT}}^{-2}$, which decreases sharply with the increasing CS-nucleus distance as the CS moves away from the NE. On the other hand, the magnitude and the scale of variation of the nuclear pulling force are found to be relatively small compared to the nuclear pushing force. As the number of MTs interacting with the nucleus ($N_{\text{MT}}^{\text{nuc}}$) decreases with the increase of the CS-nucleus distance, the nuclear pulling force decreases due to $F_{\text{pull}}^{\text{nuc}} \propto N_{\text{MT}}^{\text{nuc}}$.

To discern the combined effect of the nuclear push ($F_{\text{push(net)}}^{\text{nuc}}$) and pull ($F_{\text{pull}}^{\text{nuc}}$) on the CS positioning, all the nucleus originated forces are applied simultaneously and the centrosomal trajectory is recorded [Fig. 3(d)]. Under the influence of the resultant force ($F_{\text{total}}^{\text{nuc}}$) the CS moves to the cell membrane as it does when subjected to $F_{\text{push(net)}}^{\text{nuc}}$ alone. Thus we plot $F_{\text{total}}^{\text{nuc}}$ as a function of CS-nucleus distance in Fig. 3(e) and compare with $F_{\text{push(net)}}^{\text{nuc}}$ shown in Fig. 3(c). Interestingly, the characteristics of these two forces appear to be very similar, indicating that $F_{\text{push(net)}}^{\text{nuc}}$ completely dominates over $F_{\text{pull}}^{\text{nuc}}$ and resulting in the CS moving according to the characteristic of $F_{\text{push(net)}}^{\text{nuc}}$. To test the effect of the resultant nuclear force on the CS positioning when the nucleus is not
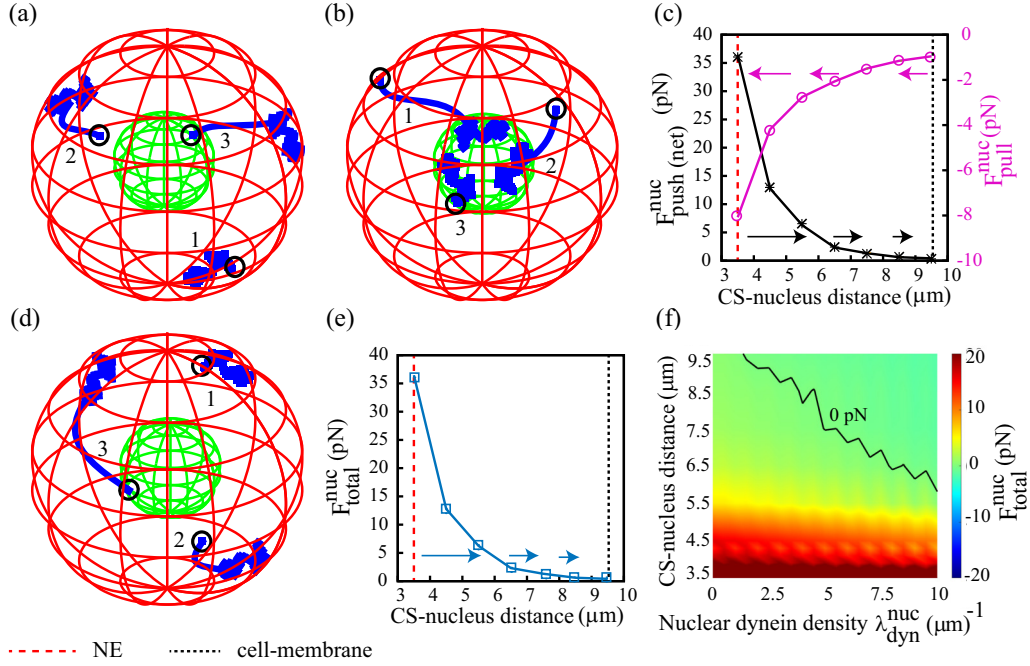
FIG. 3. Effects of the nuclear forces on the CS positioning presented as in Fig. 2. CS trajectories under these forces suggest that irrespective of the initial position, (a) CS finally reaches the cell membrane driven by nuclear pushing force, (b) CS finally lands on the NE provided nuclear pulling force is the only driving force. (c) The net nuclear pushing force, $F_{\text{push(net)}}^{\text{nuc}}$ (asterisk), falls rapidly from ~ 35 pN to zero as the distance between CS and nucleus increases and this force is directed away from the NE (rightward vector arrows). On the other hand, the nuclear pulling force, $F_{\text{pull}}^{\text{nuc}}$ (open circle), changes only marginally (~ -1 to -8 pN) and this force is directed (leftward vector arrows) toward the NE. (d) Trajectory of the CS showing the object finally moves to the cell membrane when all the nuclear forces act simultaneously. (e) The combined nuclear force on CS, $F_{\text{total}}^{\text{nuc}}$, is directed away from the NE (the rightward vector arrows) and the characteristic of this force is very similar to the characteristic of the net nuclear pushing force in (c). (f) The black line in the heat map represents the locus of the zero force region (stable fixed point) for the CS. Beyond a threshold value of the nuclear dynein density (i.e., $\lambda_{\text{dyn}}^{\text{nuc}} \simeq 2\ \mu\text{m}^{-1}$), CS leaves the cell membrane (9.5 μm line) and gradually moves toward the NE as $\lambda_{\text{dyn}}^{\text{nuc}}$ increases.

at the cell center, we put the nucleus in the off-central places of the cell and investigate $F_{\text{total}}^{\text{nuc}}$ as a function of CS-nucleus distance. We find that for any off-central position of the nucleus inside the cell, $F_{\text{total}}^{\text{nuc}}$ pushes the CS away from the NE (see Appendix D for details).

Since the nuclear dynein density on the MT is considered to be small (0.03 μm^{-1}), the pulling force is completely suppressed by the large pushing force arising from the nucleus-MT interaction. Thus, we further investigate whether an enhanced nuclear dynein density ($\lambda_{\text{dyn}}^{\text{nuc}}$) can bring any significant change in the CS position. We find that the nuclear pulling force can, in fact, neutralize the nuclear pushing force (bold line) only when the CS is far from the NE (i.e., far from the 3.5 μm line) and the nuclear dynein density is very high (i.e., $\sim 2\ \mu\text{m}^{-1} \leqslant \lambda_{\text{dyn}}^{\text{nuc}} \leqslant 10\ \mu\text{m}^{-1}$) [Fig. 3(f)]. It turns out that a properly positioned CS (~ 1–$2\ \mu$m away from the nucleus) may be achieved when $\lambda_{\text{dyn}}^{\text{nuc}}$ is extremely large ($>10\ \mu$m^{-1}) to be relevant for any realistic scenario [30,31].

C. Combined cortical and nuclear forces can stably place the centrosome in the perinuclear region

Exploring the independent effects of the resultant cortical and nuclear forces on the CS positioning [Figs. 2(d) and 2(e), and Figs. 3(d) and 3(e)], we investigate the combined effect of these two forces ($F_{\text{total}}^{\text{cor \& nuc}}$) [Fig. 4(a)]. It is observed that

$F_{\text{total}}^{\text{cor \& nuc}}$ brings the CS to the perinuclear region where the CS is able to maintain its position. To analyze this further, we plot $F_{\text{total}}^{\text{cor \& nuc}}$ as a function of CS-nucleus distance [Fig. 4(b)]. It is observed that when the CS is adjacent to the NE, $F_{\text{total}}^{\text{cor \& nuc}}$ is positive; i.e., $F_{\text{total}}^{\text{cor \& nuc}}$ pushes the CS away from the NE. $F_{\text{total}}^{\text{cor \& nuc}}$ becomes zero when the CS is $\sim 1.9\ \mu$m away from the NE and if the CS-nucleus distance increases further, $F_{\text{total}}^{\text{cor \& nuc}}$ becomes negative; i.e., $F_{\text{total}}^{\text{cor \& nuc}}$ pulls the CS toward the NE. Therefore, the zero-force region ($\sim 1.9\ \mu$m away from the NE) is a stable fixed point for the CS in the force-distance diagram in Fig. 4(b). In other words, the CS will always arrive at this perinuclear destination from any initial position inside the cell. The directional change of $F_{\text{total}}^{\text{cor \& nuc}}$ with CS-nucleus distance can be understood as follows: The CS located close to the NE (within $\sim 1.9\ \mu$m) allows a greater number of MTs to interact with the NE compared to the cortical localization resulting the nucleus-based force dominating over the cortical force; i.e., $F_{\text{total}}^{\text{cor \& nuc}}$ becomes nucleus dominated and is positive [Fig. 3(e)]. On the other hand, when the CS is away from the NE (more than $\sim 1.9\ \mu$m), more MTs interact with the cortex compared to the NE resulting the cortical force governing the CS and hence $F_{\text{total}}^{\text{cor \& nuc}}$ becomes negative [Fig. 2(e)]. The effect of the cortical and the nuclear forces on the CS is completely neutralized when the CS lies neither very close to the nucleus nor very far (interestingly within 1–2 μm away from the nucleus). To test the combined effect of the
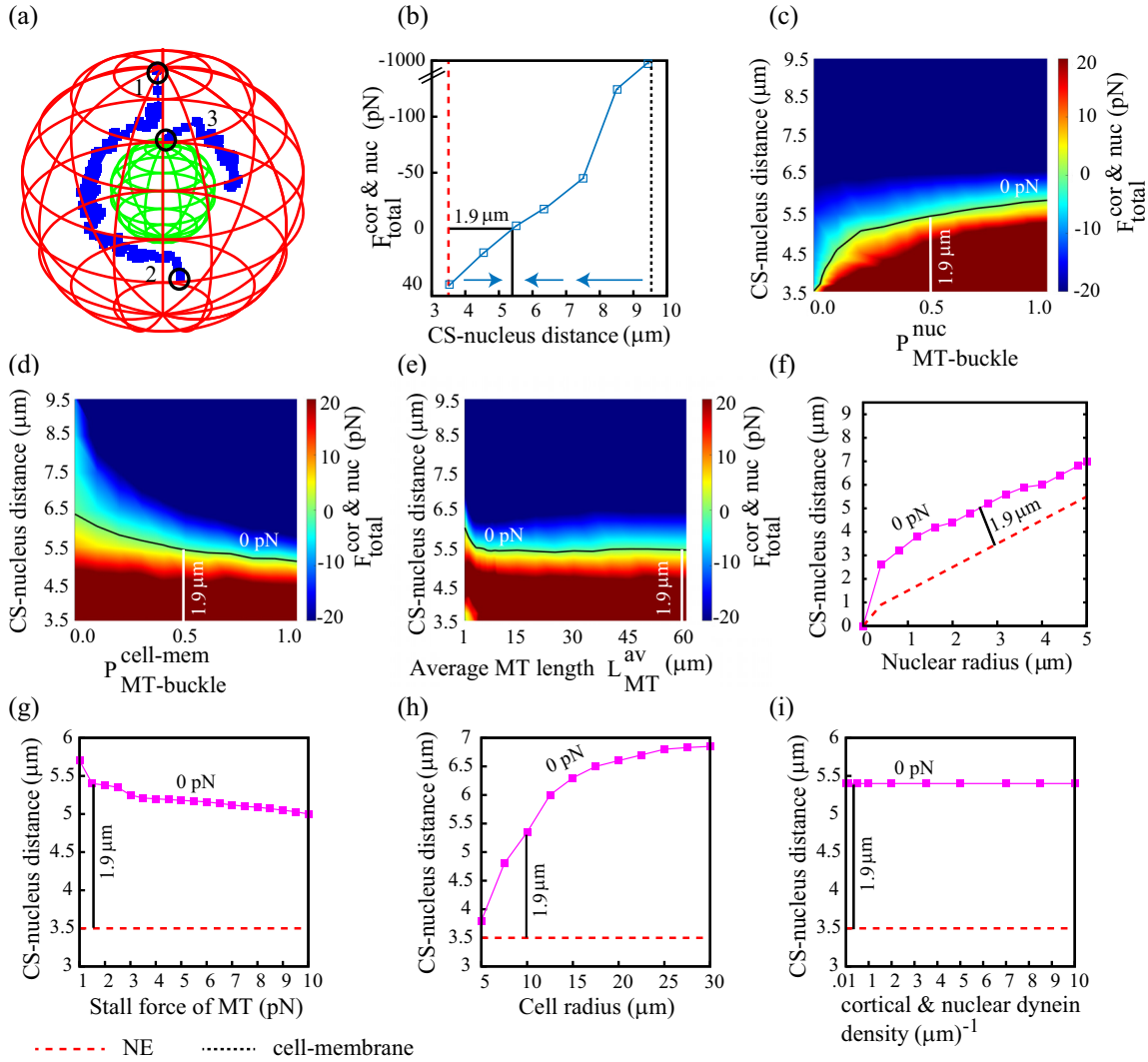
FIG. 4. The joint effect of all the cortical and nuclear forces on the CS positioning is depicted here. CS trajectories under the joint force (i.e., $F_{total}^{cor\&nuc}$) are presented following the scheme in Fig. 2. Irrespective of the initial position of the CS, (a) it finally reaches the perinuclear region and remains $\sim 1.9\,\mu$m away from the nucleus. (b) For CS distance less than $1.9\,\mu$m from the NE, $F_{total}^{cor\&nuc}$ is directed away from the NE (rightward vector arrow). The same force is directed exactly opposite, i.e., toward the NE, when CS-nucleus distance is greater than $1.9\,\mu$m. (c) With the increase of MT buckling probability at the NE, the stable fixed points for the CS (black line) gradually shift away from the NE. (d) With the increase of MT buckling probability at cell membrane, the stable fixed points for the CS (black line) gradually shift away from the cell membrane. (e) For very short MTs (i.e., $1\,\mu$m $\leqslant L_{MT}^{av} \lesssim 7\,\mu$m), the stable fixed points for the CS (black line) are shifted away from the NE. As L_{MT}^{av} increases, the stable fixed points move closer to the NE and finally maintain a separation $\sim 1.9\,\mu$m away from the NE. (f) For all nonzero values of nucleus radius, the solid data point line, i.e., the locus of the stable fixed point for the CS ($F_{total}^{cor\&nuc}$ on CS is zero), maintains a constant distance ($\sim 1.9\,\mu$m) from the NE and when the nucleus completely vanishes (nucleus radius is zero) from the cell, the CS gets the stable fixed point at the cell center (nucleus center is the cell center). (g) CS-nucleus distance upon variation in stall force of MT shows marginal change in the stable position of the CS. (h) CS-nucleus distance increases monotonically followed by a saturation as the cell size is increased. (i) CS-nucleus distance remains constant if cortical and nuclear dynein densities are varied in unison.

cortical and the nuclear forces on the CS positioning when the nucleus is not at the cell center, once again we investigate $F_{total}^{cor\&nuc}$ as a function of CS-nucleus distance (see Appendix D for details). We find that for any off-central position of the nucleus, the stable fixed point for the CS always appears in the perinuclear region. These results suggest that simultaneous application of the cortical force and nuclear forces draws the CS to the perinuclear region irrespective of the position of the nucleus.

For the sake of simplicity, we have considered 50% of the MTs hitting the NE and at the cell membrane to undergo buckling (i.e., $P_{MT-buckle}^{nuc} = P_{MT-buckle}^{cell-mem} = 0.5$). Since the MT buckling force is large, we investigate whether the fraction of the MTs buckling at the NE and at the cell membrane can bring any significant change in the characteristics of the combined force ($F_{total}^{cor\&nuc}$). To this aim, when the percentage of MT buckling at the NE ($P_{MT-buckle}^{nuc}$) is varied from 0 to 1, keeping a fixed $P_{MT-buckle}^{cell-mem} = 0.5$, the stable fixed

points for the CS position (black line) move away from the NE [see Fig. 4(c)]. It is observed that with the increase of $P_{\text{MT-buckle}}^{\text{nuc}}$, the nucleus contributed MT buckling force on the CS increases. As the nuclear MT buckling force is directed away from the NE, the CS gradually departs from the NE toward the stable fixed point. In the opposite context, when the percentage of MT buckling at the NE is kept fixed at 50% and $P_{\text{MT-buckle}}^{\text{cell-mem}}$ is increased from 0 to 1, the stable fixed point for the CS (black line) is shifted toward the NE [see Fig. 4(d)]. Clearly, as $P_{\text{MT-buckle}}^{\text{cell-mem}}$ increases, the MT buckling force on CS from the cell membrane also increases and gradually pushes the CS toward the NE.

In wild-type (WT) cells, normally, MTs go significantly long before undergoing a catastrophe. In our simulation, we have so far considered long MTs with average length $60\,\mu\text{m}$ [4,5]. MTs become fragmented upon treatment of several MT depolymerizing drugs, e.g., the nocodazole, the vinca alkaloids, or the taxanes [32] in wild-type cells, and a similar phenotype may exist naturally in specific mutants [33,34]. To explore the CS positioning in such abnormal phenotype, we investigate the feature of $F_{\text{total}}^{\text{cor \& nuc}}$ as a function of the average MT length [Fig. 4(e)]. We observe that when the MTs are very short (i.e., $L_{\text{MT}}^{av} \sim 1\text{--}7\,\mu\text{m}$), the stable fixed point for the CS is shifted farther away from the NE. As the L_{MT}^{av} is increased, the CS-NE distance starts decreasing and saturates beyond $\sim 7\,\mu\text{m}$. For very short MTs, the buckling arising due to the MT-NE interaction dominates and pushes the CS away. However, considering that the surface area of the NE is relatively small compared to the surface area of the cortex, a larger L_{MT}^{av} augments the number of MTs interacting with the cortex ($N_{\text{MT}}^{\text{cor}}$) than those interacting with the NE ($N_{\text{MT}}^{\text{nuc}}$). Consequently, the increase of the resultant cortical force on the CS [away from the cell membrane as in Fig. 2(e)] is higher than the resultant nuclear force pushing the CS away from the nucleus. Interestingly, when L_{MT}^{av} increases beyond $\sim 7\,\mu\text{m}$, the stable fixed point maintains a fixed distance of $1.9\,\mu\text{m}$ from the NE. If the MT length increases beyond $7\,\mu\text{m}$ to more, all MTs can effectively reach the cortex (i.e., L_{MT}^{av} is equivalent to the radial separation between the NE and cortex), resulting in no further change in the CS-NE distance.

To further explore the position of the CS in the absence of the nucleus and for different sizes of the nucleus, we plot the locus of the stable fixed points of the CS (i.e., when the resultant $F_{\text{total}}^{\text{cor \& nuc}}$ on the CS is zero) as a function of the nuclear radius [Fig. 4(f)]. We notice that when the nucleus is absent in the cell (i.e., nuclear radius shrinks to zero), the stable fixed point of the CS appears at the cell center (cell and the nucleus are concentric). In the absence of the nucleus, the resultant nuclear force on the CS vanishes completely and the CS is driven by the resultant cortical force only. As the resultant cortical force is directed away from the cell membrane [Fig. 2(e)], the CS gradually approaches toward the cell center and maintains the position forever. Note that in the absence of the nucleus, the central position of the CS concurs with the previous results [4,5,12,13]. In the presence of a nucleus with finite radius, we observe that the stable fixed points of the CS always appear at a constant separation ($\sim 1.9\,\mu\text{m}$) away from the NE. Thus, irrespective of the size of the nucleus, the CS always remains in the perinuclear region a finite distance away from the NE.

We also explore the separation between the CS and the nucleus as a function the stall force of the MT [Fig. 4(g)], size of the cell [Fig. 4(h)], and dynein density at the cortex and NE [Fig. 4(i)]. We find that the CS-nucleus distance changes marginally as the stall force of the MT is increased. Next, we vary the cell size keeping the nuclear radius (r_{nuc}) constant at $3\,\mu\text{m}$ and observe a rapid increase in the CS-nucleus separation. This happens due to the decrease in the MT population reaching the cortex (owing to a larger cell radius) resulting in a reduction in the net pushing force applied on the CS originating from the cortex. However, after a certain size of the cell, the net pushing force from the cortex changes marginally leading to a slow variation in the CS-nucleus separation. Further we observed that upon variation in the dynein densities in cortex and NE equally, the CS-nucleus separation remains unaltered.

VI. ANALYTICAL PRESCRIPTION IN 1D

Here we propose a simplistic mathematical model (see Appendix B for details), taking into account all major MT mediated force contributions from the cortex and the nucleus on the CS, in order to investigate various regimes in the force balance landscape optimally leading to the proper CS positioning. In the following, we explicitly describe and compare our analytical findings regarding the combinatory effects of various forces, namely pushing, pulling, and buckling originating at the cortex and NE [Figs. 5(a)–5(f)] with the simulation outcomes elucidating the spatiotemporal dynamics of the CS under the concerted or opposing efforts of MT pushing, pulling, and buckling stemming from the cortex and NE [Figs. 6(a)–6(d)].

A. Cortical (nuclear) push concurrently with cortical (nuclear) pull cannot orchestrate proper centrosome positioning in the perinuclear region

It is evident from Fig. 5(a) (solid line) that for large average MT length ($L_{\text{MT}}^{av} \sim 60\,\mu\text{m}$) there is a tug of war between these two competing forces which determines the "stable" location of the CS. For small cortical dynein density ($\lambda_{\text{dyn}}^{\text{cor}}$), net cortical push dominates over cortical pull and shoves the CS onto the nucleus. A slight increase in the cortical dynein density leads to a sharp transition to a cortical pull dominated regime where the CS stays close to the cell periphery. It is very unlikely to capture this "sharp" spatial changeover of the CS from the nucleus to the cell periphery within the cell owing to the ambient noise and other relevant factors in the cytoplasm. However, the proposed competing behavior between cortical pushing and pulling in the CS positioning still holds qualitatively. We investigate this proposition in our 3D simulation [Fig. 6(a)] (open square line) and observe a qualitatively same outcome. Here, for $L_{\text{MT}}^{av} \sim 60\,\mu\text{m}$, an interplay occurs between the cortical push and the cortical pull and the cortical pull completely dominates over the cortical push when the dynein density at the cortex becomes high ($0.3\,\mu\text{m}^{-1}$).

In the absence of the cortical forces, the sole presence of the nuclear push nudges the CS toward the cell membrane. In Fig. 5(a) (dot-dashed line), as the dynein activity on the NE is gradually increased, nuclear pushing loses against a
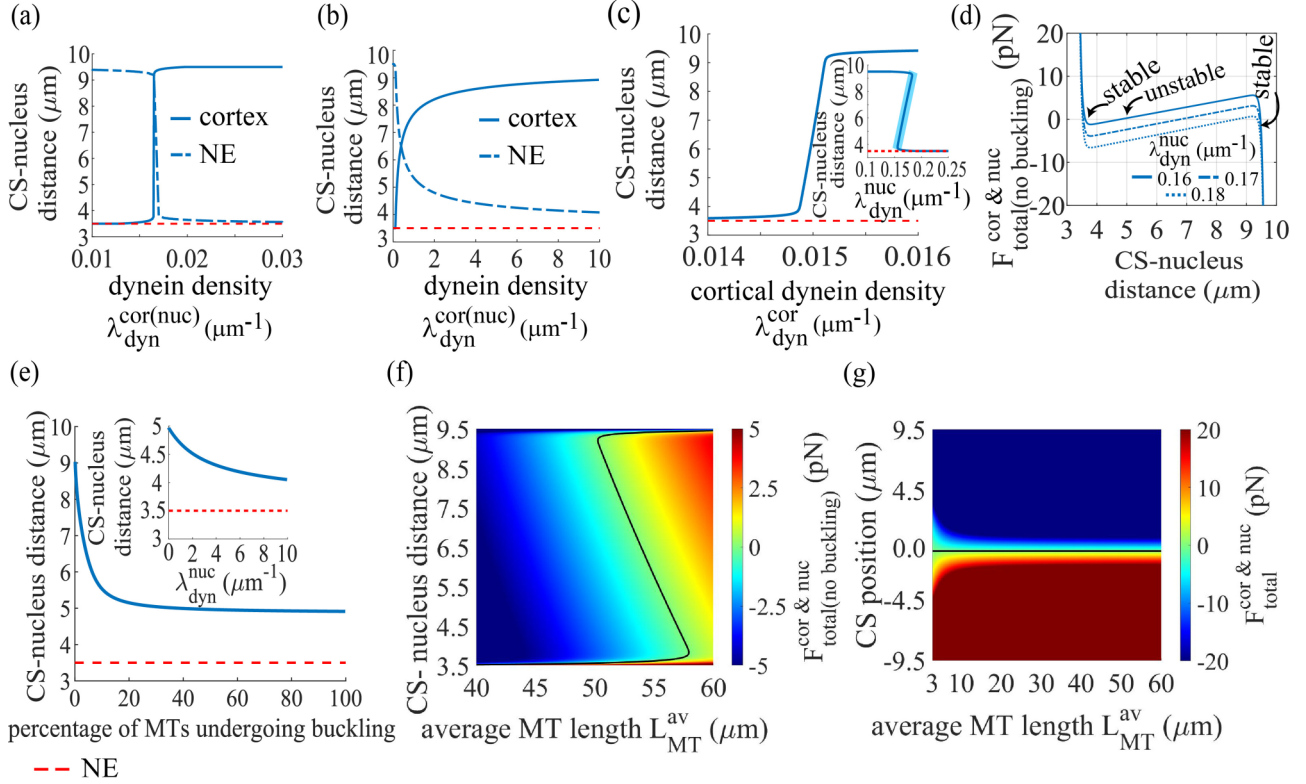
FIG. 5. MT mediated force balance landscape determining CS positioning in the presence of a myriad of cortical and nuclear determinants (analytic description in 1D). (a) Variation of cortical (nuclear) dynein density ($\lambda_{dyn}^{cor(nuc)}$) initiates a spatial changeover in CS positioning. Solid (dot-dashed) line depicts the presence of mutually competing instantaneous cortical (nuclear) push and dynein mediated cortical (nuclear) pull only. The y labels at 3.5 μm and 9.5 μm mark the position of NE and cell membrane, respectively. (b) In the presence of MT buckling transition the CS stabilizes ~0.5 μm away from the cell membrane (NE) at a higher dynein density [λ_{dyn}^{cor} (λ_{dyn}^{nuc}) $\geqslant 4.0$ μm^{-1}]. Solid (dot-dashed) line depicts the presence of instantaneous cortical (nuclear) push, cortical (nuclear) buckle, and cortical (nuclear) pull. (c) Locus of the fixed point upon the variation of cortical dynein density when instantaneous cortical push, cortical pull, and instantaneous nuclear push act in tandem. Inset: Gradual increase in nuclear dynein density (λ_{dyn}^{nuc}) at a fixed value of $\lambda_{dyn}^{cor} = 0.03$ μm^{-1} brings over the CS in the vicinity of NE via a string of unstable fixed points when instantaneous cortical push and pull act in harness with nuclear push and pull. (d) Spatial profile of the net force on CS elucidating stable and unstable fixed points. (e) Variation in the percentage of MTs undergoing buckling at cell membrane and NE over a large range does not alter the perinuclear positioning of the loci of stable fixed points for the CS in the presence of instantaneous cortical push, cortical pull ($\lambda_{dyn}^{cor} = 0.03$ μm^{-1}) in tandem with instantaneous nuclear push. Inset: Variation in nuclear pull (λ_{dyn}^{nuc}) in the presence of cortical push, pull ($\lambda_{dyn}^{cor} = 0.03$ μm^{-1}), and buckle (50%) in tandem with nuclear push and buckle (50%) does not alter the CS localization significantly. (f) String of unstable fixed points under the presence of instantaneous push and dynein pull from cortex and NE ($\lambda_{dyn}^{cor} = 0.03$ μm^{-1}, $\lambda_{dyn}^{nuc} = 0.15$ μm^{-1}) upon variation in average MT length (L_{MT}^{av}) when MT buckling transition at cortex and NE is absent. (g) CS localizes at cell center in the absence of the nucleus.

heightened nuclear pull, leading to a collapse of the CS onto the NE. The respective simulation outcome [Fig. 6(a)] (open circle line) runs parallel with this finding in a qualitative manner.

B. In the absence of cortical forces MT buckling at the NE concomitantly with nuclear push and pull prevent the centrosome from collapsing onto the nucleus

In reference to Fig. 5(b) (solid line), we have considered that the total number MTs hitting the cortex is 50 with a weight $e^{-(r_{cell}-x)/L_{MT}^{av}}$. Out of all these MTs hitting the cortex, 50% are undergoing sliding and the rest are undergoing buckling. Usually, the force generated due to a single MT buckling

goes as $\pi^2 k_B T L_p / L^2$, where L_p is the persistence length of the MT [5,35].

It is evident from Fig. 5(b) (solid line) that upon stepwise increase in the cortical dynein density (λ_{dyn}^{cor}) the stable fixed point of the CS undergoes a sharp spatial changeover from the NE to cell membrane. Unlike Fig. 5(a), the string of stable fixed points at higher λ_{dyn}^{cor} ($\geqslant 4$ μm^{-1}) does not lie exactly on the cell membrane, but ~0.5 μm away from the cell membrane. For MT bending rigidity ($\pi^2 k_B T L_p$) times the number of MTs undergoing buckling ($D \sim 200 \times 25$ pN μm^2) [5], $F_{MT-buckle}^{cell-mem}$ imparts a strong short range pushing force upon the CS in the vicinity of the cell membrane which prevents the CS from collapsing onto the cell membrane. In Fig. 6(b) (open square line), the respective simulation outcome is depicted, where the move of the stable fixed point

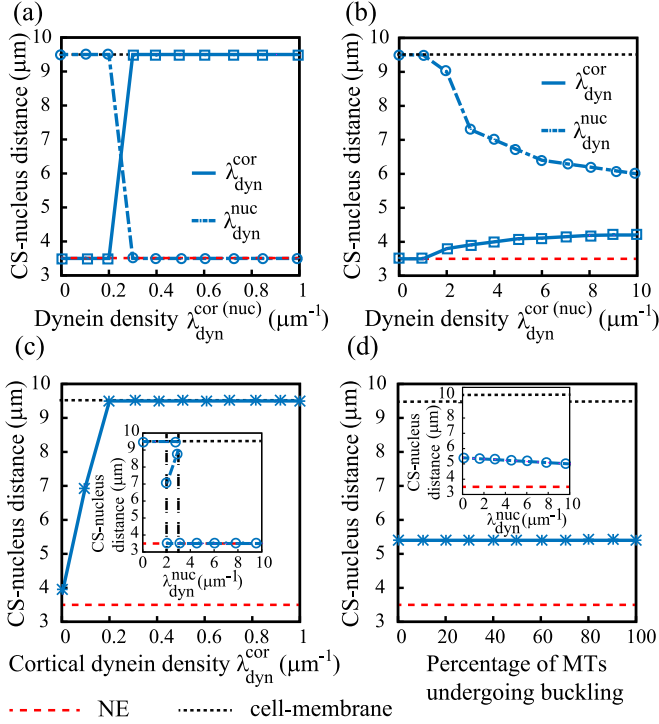- - - - - NE   ········· cell-membrane

FIG. 6. MT mediated force balance landscape determining CS positioning in the presence of a myriad of cortical and nuclear determinants (description with simulation results in 3D). (a) Variation of cortical (nuclear) dynein density ($\lambda_{dyn}^{cor(nuc)}$) initiates a spatial changeover in CS positioning. Solid (dot-dashed) line depicts the presence of mutually competing instantaneous cortical (nuclear) push and dynein mediated cortical (nuclear) pull only. (b) In the presence of the MT buckling transition the CS stabilizes $\sim 5.3\,\mu$m ($\sim 2.5\,\mu$m) away from the cell membrane (NE) at a very high dynein density [λ_{dyn}^{cor} (λ_{dyn}^{nuc}) $= 10\,\mu$m^{-1}]. Solid (dot-dashed) line depicts the presence of instantaneous cortical (nuclear) push, cortical (nuclear) buckle, and cortical (nuclear) pull. (c) Locus of the fixed point upon the variation of cortical dynein density when instantaneous cortical push, pull, and nuclear push act in tandem. Inset: Gradual increase in nuclear dynein density (λ_{dyn}^{nuc}) at a fixed value of $\lambda_{dyn}^{cor} = 0.03\,\mu$m^{-1} brings over the CS in the vicinity of NE via a string of unstable fixed points when instantaneous cortical push and pull act in harness with nuclear push and pull. (d) Variation in the percentage of MTs undergoing buckling at cell membrane and NE over a large range does not alter the perinuclear positioning of the loci of stable fixed points for the CS in the presence of instantaneous cortical push, cortical pull ($\lambda_{dyn}^{cor} = 0.03\,\mu$m^{-1}) in tandem with instantaneous nuclear push. Inset: Variation in nuclear pull (λ_{dyn}^{nuc}) in the presence of cortical push, pull ($\lambda_{dyn}^{cor} = 0.03\,\mu$m^{-1}), and buckle (50%) in tandem with nuclear push and buckle (50%) does not alter the CS localization significantly.

toward the cell membrane is very slow with the increase of λ_{dyn}^{cor}. Upon stepwise increase in nuclear dynein density λ_{dyn}^{nuc}, owing to strong pull from the nucleus in the absence of cortical forces ($\lambda_{dyn}^{nuc} \geqslant 4\,\mu$m^{-1}), the string of stable fixed points localizes in the proximity of the NE [Fig. 5(b), dot-dashed line]. The respective simulation outcome [Fig. 6(b)] (open circle line) also indicates that when the cortical forces are absent, the stable fixed point for the CS gradually moves toward the NE with the increase of λ_{dyn}^{nuc}.

C. Interplay among cortical push and pull in harness with nuclear push and pull leads to a string of unstable fixed points during the spatial changeover of the centrosome

According to the default model construction, the nuclear push is positive and acts in concert with the cortical pull to move the CS toward the cortex. Hence in Fig. 5(c), under the influence of the cortical push, the pull in concert with nuclear push, the location of the stable fixed points for the CS makes a changeover from the NE to the cell membrane at a slightly lower λ_{dyn}^{cor} compared to Fig. 5(a), and the slope of the changeover flattens out to a small extent owing to the presence of nuclear push effectively enhancing the net force toward the cell membrane. When $\lambda_{dyn}^{cor} \sim 0.015\,\mu$m^{-1}, the stable fixed point for the CS is $\sim 2\,\mu$m away from the NE. The presence of this stable point denotes that the CS does not plunge into the nucleus but stalls at a stable position close to the nucleus. In the absence of nuclear pull, at $\lambda_{dyn}^{cor} \geqslant 0.0155\,\mu$m^{-1}, the CS stays in the proximity of the cell membrane. Strikingly, upon gradual increase in λ_{dyn}^{nuc} at a higher value of λ_{dyn}^{cor} ($\sim 0.03\,\mu$m^{-1}) the stable fixed point leaps from the cell membrane to the NE [Fig. 5(c), inset] marked by a small region (0.15 μm$^{-1} \leqslant \lambda_{dyn}^{nuc} \leqslant 0.20\,\mu$m^{-1}) where the CS has two stable fixed points at the cell membrane and the NE, respectively, and an unstable fixed point slotted in between. The unstable fixed point denotes that the CS when slightly displaced from that location plunges either onto the cell membrane or onto the NE depending upon the direction of the perturbation [Fig. 5(d)]. This analytic prescription is consistent with our simulation outcome [see Fig. 6(c)].

D. Cortical push, pull, and buckle in harness with nuclear push, pull, and buckle properly localize the centrosome in the perinuclear region

In the absence of the nuclear pull, we obtain a stable fixed point for the CS $\sim 1.5\,\mu$m away from the NE [Fig. 5(e)], when $\geqslant 15\%$ MTs are undergoing the buckling transition and the rest of the MTs are sliding (other parameters: $A = $ [total number of MTs at cortex (NE) $-$ number of buckling MTs at cortex (NE)] pN, $B = $ [total number of MTs at cortex (NE) $-$ number of buckling MTs at cortex (NE)] pN, $D = $ (number of MTs) $\times \pi^2 k_B T L_p / L^2 \simeq 200 \times$ (number of buckling MTs) pN μm^2, $\lambda_{dyn}^{cor} = 0.03\,\mu$m^{-1}). In this parameter regime, it is also evident that substantial variation in nuclear pull (0.0 μm$^{-1} \leqslant \lambda_{dyn}^{nuc} \leqslant 10.0\,\mu$m^{-1}) does not alter the location of the fixed point significantly [Fig. 5(e), inset]. It is evident that force due to buckling shoots up to a very high value ($\sim 10^3$ pN) and it is no longer short range, thereby spanning all the accessible values of CS-nucleus distance [Fig. 5(e)]. In this scenario if the probability of MTs undergoing buckling is $\geqslant 20\%$, the loci of stable fixed points for the CS evidently maintains a constant 1.5 μm distance away from the NE [Fig. 5(e), inset]. CS positioning via this mechanism is not significantly sensitive to dynein mediated pull from nucleus.

The respective simulation outcome [Fig. 6(d)] also introduces the fact that in the absence of the nuclear pull, the stable fixed point for the CS appears $\sim 2.0\,\mu$m away from the NE, when 50% of MTs are undergoing the buckling transition and rest of the MTs are sliding (other parameter:

$\lambda_{\text{dyn}}^{\text{cor}} = 0.03 \ \mu\text{m}^{-1}$). Here, the location of the fixed point is not shifted significantly with the increase of $\lambda_{\text{dyn}}^{\text{nuc}}$ (inset).

In the absence of the MT buckling transition we obtain CS localization profiles with three fixed points (two stable fixed points at the cortex and NE and another unstable fixed point sandwiched in between) over a significant variation in average MT length (L_{MT}^{av}; other parameters: $\lambda_{\text{dyn}}^{\text{cor}} = 0.03 \ \mu\text{m}^{-1}$, $\lambda_{\text{dyn}}^{\text{nuc}} = 0.15 \ \mu\text{m}^{-1}$), which is evident from the "inverted Z" contour [Fig. 5(f)].

In the presence of the MT buckling transition and instantaneous push along with the dynein pull from the cortex and NE the respective force balance leads to a stable CS localization at the cell center [Fig. 5(g)] owing to the intrinsic symmetry of the confinement under consideration.

In most of the cases the findings from the 2D mathematical description of the CS positioning closely corroborate the 1D description [Figs. 7(a)–7(d)]. From Figs. 5(d) and 7(d), we glean that the net buckling force at the cortex in 2D is relatively higher due to the increased cortical surface area accessible by the MTs in the 2D construction compared to the earlier 1D build-out. Strikingly, in the currently explored parameter regime we do not obtain any unstable fixed point across the force balance landscape, unlike the 1D description.

In this report, we have also explored the 1D force balance landscape for CS positioning in the presence of short MTs (see Appendix E for details).

VII. DISCUSSION

A prerequisite for the formation of mitotic spindle architecture is the positioning of the centrosome (CS) in the proximity to the nuclear surface. Spatiotemporal maintenance of the CS position requires a mechanical force balance on the CS arising out of a concerted interplay between a myriad of molecular motors (e.g., dynein) and microtubule (MT) mediated force generating (transmitting) machineries. Our study sheds light on the mechanistic context of perinuclear positioning of the CS taking into account major MT mediated force contributions from the cortex and the nucleus in a nonpolarized cell.

We undertook a reductionist approach while building up the computational and mathematical model. The theoretical underpinnings of the model framework are based on a number of assumptions described in the preceding sections. However, like any other theoretical model, this model accounting for the perinuclear positioning of the CS does not explicitly mimic the reality. Rather this setup replicates the "jiggling and wiggling" of the cellular components under consideration to a reasonably good approximation with certain limitations described in the following.

(1) In the model the stochastic effects are incorporated in the MT dynamics in terms of catastrophe and rescue frequency. A growing MT stochastically switches to the shrinking state and vice versa being subjected to the predetermined catastrophe and rescue frequency or rate. The stochasticity at the molecular level during MT polymerization or depolymerization is not considered in the model. In the mathematical model, the intrinsic stochasticity is marked by the exponential distribution function governing the MT lengths. In the model, when the MT reaches the cortex or NE, the MT either slides
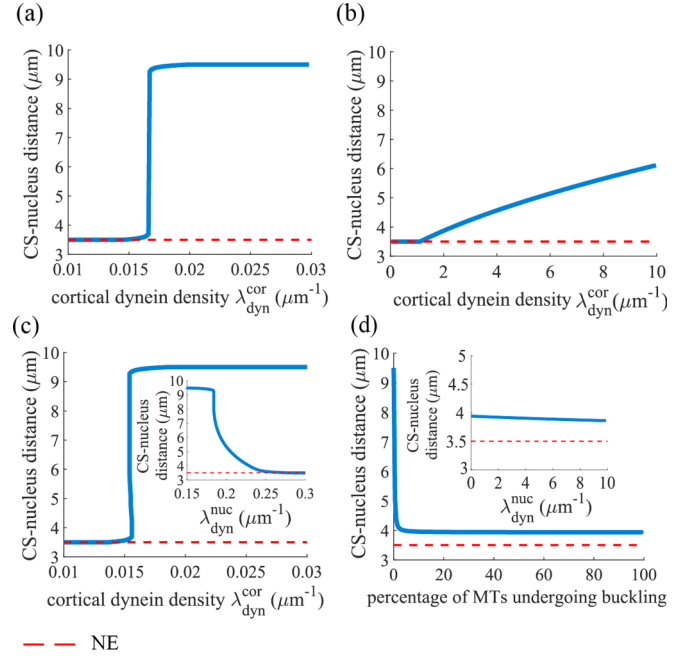

FIG. 7. Force balance landscape for CS positioning derived from 2D mathematical prescription. For all the following figures, the y labels at 3.5 μm and 9.5 μm mark the position of NE and cell membrane, respectively. (a) Variation of cortical dynein density initiates a "sharp" spatial changeover in CS positioning in the presence of mutually competing instantaneous cortical push and dynein mediated cortical pull. (b) In the presence of MT buckling transition at the cell membrane along with cortical push and pull, upon gradual increase in cortical dynein density $\lambda_{\text{dyn}}^{\text{cor}}$ the CS position slowly moves toward the cell membrane instead of a "sharp" spatial changeover. (c) Loci of fixed points upon the variation of cortical dynein density when instantaneous cortical push, pull, and nuclear push act in tandem. Inset: Gradual increase in nuclear dynein density ($\lambda_{\text{dyn}}^{\text{nuc}}$) at a fixed value of $\lambda_{\text{dyn}}^{\text{cor}} = 0.03 \ \mu\text{m}^{-1}$ brings over the CS in the vicinity of NE. (d) Variation in the percentage of MTs undergoing buckling at cell membrane and NE over a large range does not alter the perinuclear positioning of the loci of stable fixed points for the CS in the presence of instantaneous cortical push, cortical pull ($\lambda_{\text{dyn}}^{\text{cor}} = 0.03 \ \mu\text{m}^{-1}$) in tandem with instantaneous nuclear push. Inset: Variation in nuclear pull ($\lambda_{\text{dyn}}^{\text{nuc}}$) in the presence of cortical push, pull ($\lambda_{\text{dyn}}^{\text{cor}} = 0.03 \ \mu\text{m}^{-1}$ and $\tilde{B} = 0.5$ pN), and buckle (50%) in tandem with nuclear push and buckle (50%) ($\tilde{D} = 0.5 \times 200$ pN μm^2) does not alter the CS localization significantly.

along the cortex or undergoes the buckling transition with the MT tip pivoted at the cell membrane. This decision making (whether the MT undergoes sliding or buckling) is also stochastic being subjected to predetermined rates which we varied as a parameter in the system. However, stochastic effects regarding the binding or unbinding of dyneins on MT tracks resulting in fluctuations in force generation are neglected for simplicity. The randomness and temperature fluctuation originating from the embedding viscous fluid (e.g., the cytoplasm) are also not considered.

(2) The consideration of the fact that the nucleus and the cell are not spherical will lead to significant changes in the force balance landscape and the symmetry arguments in the mathematical prescription will have to be revisited. For

example, if we consider an ellipsoidal nucleus within a spherical cell and the CS is positioned at a location perpendicular to the major axis of the nucleus, the MTs emanating out of the CS will be exposed to a larger surface area of the NE that in turn will shoot up the net force contribution from the NE. On the contrary, if the CS is placed at a location perpendicular to the minor axis of the nucleus, the net force contribution from the NE will be lesser than the earlier configuration, since the surface area of the NE exposed to the MT "shower" is reduced. The consideration of an ellipsoidal cell and a spherical nucleus will also impose similar anisotropy-induced changes in the cortical force contributions.

(3) MT entanglement with the actin meshwork might play a significant mechanistic role in the perinuclear positioning of the CS. The latest report [37] suggests that the increase in centrosomal actin leads to a reduction in MT population nucleating from the CS. Interestingly, lymphocyte activation is marked by a reduction in centrosomal actin disassembly and increase in MT number. The previous report [37] postulates that actin filaments near the CS negatively regulate MT growth by posing steric hindrance. Spatial organization of MT arrays is largely regulated by the mechanistic crosstalk of MTs with actin based architecture [38,39]. Recent works reveal that the CS also serves as an actin organizing center and the physical separation between the CS and the NE increases upon the disruption of centrosomal F actin referring to a fact that centrosomal F actin is also a key player in orchestrating the tethering of the CS on the NE [40,41]. Apart from the crosstalk between centrosomal actin and MTs, there also exists a plausible mechanistic interaction between MTs and cortical actin where a myriad of forces generated due to MT sliding, buckling, etc., can be influenced by the heterogeneity in local cortical actin architecture. It is also reported that cell adhesion and spreading result in lower actin densities which in turn engineers a higher MT growth from the CS. Incorporating cellular adhesions and spatiotemporal organization of the actin meshwork in the current model taking cue from the previous experimental studies would be interesting to delve into.

(4) From the mathematical model [Eqs. (4) and (5)] we glean that the net pulling forces from the cortex and the NE are proportional to both the number of MTs (manifested in B) and linear dynein density at the cortex (NE) $\lambda_{\text{dyn}}^{\text{cor}}$ ($\lambda_{\text{dyn}}^{\text{nuc}}$). In a phase space spanned by the number of MTs ($B \propto$ number of MTs) and $\lambda_{\text{dyn}}^{\text{cor}}$ or $\lambda_{\text{dyn}}^{\text{nuc}}$, the constant force contours at a particular CS location x will trace out hyperbolae in the relevant parameter landscape. This signifies that as long as the product of the number of MTs and $\lambda_{\text{dyn}}^{\text{cor}}$ ($\lambda_{\text{dyn}}^{\text{nuc}}$) is conserved, the stable and unstable fixed points in the force balance landscape in the presence of pulling forces will remain unaltered if other parameters are kept unchanged. However, from a physical point of view, the variation in dynein mediated force generation is subjected to the on and off rates of dyneins, steric effects in loading and motor walking, MT dynamic instability, and other factors. Henceforth the theoretical prediction regarding the exact fate of the positioning in the presence of a significantly small or large number of MTs and small or large number of dyneins remains partially inconclusive. Thus, we refer to the regulation of the optimized MT and dynein density acting as a limiting factor in perinuclear positioning in realistic scenarios.

Previous studies highlighted the context of ample force generation leading to local deformations by the CS docked near the "nuclear indentation" [14,42]. Even though our model considers a "hard ball" nucleus, the force balance landscape reveals that in the presence of the MT buckling transition [with the MT bending elasticity or rigidity characterized by $D \sim 200$ pN μm^2 per MT [5] times the number of MTs hitting the cortex and NE (D'); Eq. (6) and Eq. (7)], a robust balancing act between cortical and nuclear forces fosters very stable CS-nucleus engagement sustained across large variations in percentage of MT buckling and nuclear dynein pull [Figs. 5(d) and 6(d)] where allowing deformations of the NE would not qualitatively alter the perinuclear localization. However, if we choose MT bending rigidity D to be ~ 1 pN μm^2 times the number of buckling MTs [Eq. (6), Eq. (7)], the proper perinuclear positioning occurs only when there is a moiety division among the MTs undergoing buckling and sliding, respectively. In the absence of buckling the entire force balance landscape plummets down to a low force regime where an array of unstable fixed points emerges in the spatial profile of "zero force" contours of the CS across a certain range of dynein density and average MT length [Figs. 5(c), 5(e), and 6(c)]. For shorter MTs, a string of additional unstable fixed points appears in the presence of instantaneous cortical (nuclear) push and dynein pull unlike the scenario with longer MTs [Fig. 5(a)] (see Appendix E for details). When the average MT length is drastically shortened (Appendix E), the corresponding landscape of $F_{\text{total}}^{\text{cor \& nuc}}$ (in the absence of MT buckling) undergoes a transition from a "pushing" dominated regime (net positive force) to a small window of the "pulling" dominated regime (net negative force) which in turn contributes to the "relatively" enhanced number of unstable fixed points within the explored domain of the parameter space. Previous studies [14,43,44] prescribe a two-step model for centrosome-nucleus attachment. One pathway involves translocation of the CS toward the NE via the dynein-ZYG12 complex tethered at the NE. The other pathway involves homotypic interaction of ZYG12 molecules at the NE and CS that "hooks" the CS on the NE. Our present study qualitatively captures the attributes of the former mechanism in detail.

The most notable outcome of this study is that irrespective of the size and the position of the nucleus in the cell, the CS always comes to the perinuclear region under the combined effort of the cortical and nuclear forces [Figs. 4(a), 4(b), and 4(f)] (see Appendix D for details). Therefore, the role of this combined force to the CS positioning is undoubtedly very effective and future studies on it could explore the picture further. In our present model, we have considered the static nucleus; i.e., the nucleus position is not affected by the MT mediated forces acting over the NE. Though the nucleus is very massive and moves through the highly viscous cytoplasm very slowly, the consideration of the dynamic nucleus can be an interesting further step to the study of CS positioning.

Schmoranzer and his co-workers [45] show that the concerted activities of Par3 and dynein together contribute to the proper CS positioning in migrating cells. Also in migrating neurons (specifically neurites that mature into axons), it is reported that the CS is positioned ahead of the nucleus [14,46]. Another interesting aspect of CS positioning is force

transduction via MT interaction with dyneins tethered to the cytoplasmic side of nuclear pore complexes (NPCs) within the CS-nucleus "tight pair" [47] leading to NE breakdown [48]. The present model, having a static nonpolarized cell, could further be extended to incorporate these details in a future study. Another interesting avenue to be investigated would be the spatiotemporal trajectory of the CS-nucleus assembly as a whole after the "off-centered" perinuclear localization where the nucleus is initially located randomly within cells with different shapes and sizes. Our current model could also be extended to investigate the centering of embryonic centrosomes by "cytoplasmic pulling" as a consequence of cargo transport via cytoplasmic dyneins [49]. Proper positioning of the CS also facilitates timely capture of kinetochores by astral MTs in dividing cells [43], a failure of which leads to various defects due to unequal segregation. Our current model can offer a comprehensive mechanistic perspective in elucidating these important cellular functions across different organisms in a context dependent manner.

In the light of recent experiments, we glean that the MT-actin crosstalk plays an important role in the proper positioning of the CS. Further biophysical experiments in that direction would help to validate (contradict) various aspects of mechanistic force balance obtained from our theoretical study. We have mathematical models in 1D and 2D and a computational model in 3D. It would be interesting to explore the perinuclear positioning in cells of different shapes and sizes in 2D and 3D and determine the role of dimensionality of the confinement in the whole process.

APPENDIX A: DETAILED DESCRIPTION OF 3D COMPUTATIONAL MODEL

We propose a computational model in three spatial dimensions (3D) to study the effects of various molecular forces on the positioning of the CS in a mammalian interphase cell.

a. Designing the cell, the nucleus, the centrosome, and the MTs

We consider the cell, nucleus, and CS as 3D spheres (Fig. 1) having rigid surfaces and radii r_{cell}, r_{nuc}, and r_{CS}, respectively. The steric force between the CS and the cellular or nuclear surface keeps the CS within the cytoplasm. The MTs are assumed to be semiflexible polymers undergoing dynamic instability characterized by growth velocity v_g, shrink velocity v_s, catastrophe frequency f_c, and rescue frequency f_r [4]. Under a load force $\vec{f}_{load}$, the growth velocity and the catastrophe frequency of the MTs are modified in the following manner [5]: (1) $v_g = v_{g0} \exp(-|\vec{f}_{load}|/f_{stall})$, where v_{g0} is the unconstrained growth velocity when no load is applied to the MTs, $|\vec{f}_{load}|$ is the magnitude of the load force acting along the MT in the direction opposing the MT growth,

and f_{stall} is the magnitude of the stall force of a single MT; (2) $f_c = f_c^{stall}/\{1 + [(f_c^{stall}/f_{c0} - 1) \exp(-|\vec{f}_{load}|/f_{stall})]\}$, where f_c^{stall} is the rate of catastrophe of a stalled MT and f_{c0} is the catastrophe rate of a free MT. In our study, we consider 100 MTs that are nucleated from the CS uniformly.

b. MT-cortex interaction forces on the centrosome

Interactions of the MTs with the cell cortex and membrane generate mechanical forces on the MT tips that are finally transmitted to the CS. For the sake of simplicity, we ignore the encounter angle at which the MTs impinge upon the cell cortex and membrane while calculating the forces. Thus the direction of the force is always along the length of the MT filament (Fig. 1). The direction of growth for each MT in space is designated by three direction cosines (along the x, y, and z axes) which are used to calculate the components of the forces (acting on the CS) along the x, y, and z axes. As the pushing force opposes the MT to grow further, it is considered as the load force ($|\vec{f}_{load}|$). Here we explicitly describe the mechanisms by which these forces are incorporated in the model (Fig. 1): (1) When MT polymerization is resisted by the cortical substances (adjacent to the cell membrane), a pushing force (springlike force) appears on the MT tip [21,22] denoted by $|\vec{f}_{MT-grow}^{cor}| = l_{MT}^{cor} k_{cor}$. In other words, $\vec{f}_{MT-grow}^{cor}$ is the pushing due to a single MT and $\vec{F}_{MT-grow}^{cor} = \sum_{MTs} \vec{f}_{MT-grow}^{cor}$ is the net pushing force on the CS; l_{MT}^{cor} is the segment of the MT penetrating into the cortex. This penetrated segment of the MT inside the cortex imparts a Hookean force (with effective spring constant k_{cor}) on the MT tip directed toward the CS. (2) When the polymerizing MT hits the cell membrane, an instantaneous pushing force is applied to the MT tip denoted by $|\vec{f}_{MT-hit}^{cell-mem}| = 1.0$ pN [23], and the resultant instantaneous pushing force on CS is $\vec{F}_{MT-hit}^{cell-mem} = \sum_{MTs} \vec{f}_{MT-hit}^{cell-mem}$. (3) A pulling force is applied on the MT toward the cell membrane when cortical dyneins move toward the negative end of the MT track [24,25] denoted by $|\vec{f}_{dyn}^{cor}| = l_{MT}^{cor} \lambda_{dyn}^{cor} f_{dyn}^s$, where λ_{dyn}^{cor} is the linear dynein density on the MT track inside the cortex, f_{dyn}^s is the force produced by a single dynein motor, and the resultant force on CS is $\vec{F}_{dyn}^{cor} = \sum_{MTs} \vec{f}_{dyn}^{cor}$. The above forces are further supplemented by a growing MT buckling (determined by a probability $P_{MT-buckle}^{cell-mem}$) in contact with the cell membrane or sliding (determined by a probability $P_{MT-slide}^{cell-mem} = 1 - P_{MT-buckle}^{cell-mem}$) along the cell membrane. For a buckled MT (we always consider first order Euler buckling), a large pushing force is generated on the CS away from the cell membrane along the line joining the MT tip and the CS. Once again, the interaction angle between the MT tip and the cortex is ignored while estimating the force on the CS. Since the buckling force is a pushing force applied on the MT tip, it is also considered as the load force to the MT. In this study, we denote this buckling force by $\vec{f}_{MT-buckle}^{cell-mem}$ and $|\vec{f}_{MT-buckle}^{cell-mem}| = D/l_{MT}^2$, where D is the flexural rigidity of the MT ($\sim$200 pNμm^2), l_{MT} is the instantaneous MT length, and the resultant buckling force on CS is $\vec{F}_{MT-buckle}^{cell-mem} = \sum_{MTs} \vec{f}_{MT-buckle}^{cell-mem}$ [26,27]. Since the Euler buckling force is relatively large compared to other forces in action, f_c of the buckled MT increases dramatically. In the case of sliding MTs, a large pulling force is applied on the CS toward the

cell membrane due to dynein accumulation along the sliding segment of the MT. Note that this pulling force due to sliding (a contribution to $\vec{f}_{dyn}^{cor}$) acts on the CS along the line joining the CS and the MT segment entering into the cortex from cytoplasm.

c. MT-nucleus interaction forces on the centrosome

The nucleus is a massive object and assumed to be static at the center of the cell during the interphase. From a mechanistic point of view, MTs interact with the nuclear membrane in a manner similar to that with which they interact with the cell membrane. The existing literature [19,20] suggests that the CS experiences mechanical forces when the CS-nucleated MTs interact with the nucleus. In this study, we incorporate the MT-nucleus interactions (Fig. 1) as follows: (1) When a growing MT hits the nuclear membrane, an instantaneous pushing force is generated on the MT tip denoted by $|\vec{f}_{MT-hit}^{nuc}| = 1.0$ pN and therefore the resultant force is $\vec{F}_{MT-hit}^{nuc} = \sum_{MTs} \vec{f}_{MT-hit}^{nuc}$. (2) After hitting the nuclear membrane, the growing MT either buckles in contact with the membrane (determined by a probability $P_{MT-buckle}^{nuc}$) or slides along the nuclear membrane (determined by a probability $P_{MT-slide}^{nuc} = 1 - P_{MT-buckle}^{nuc}$). In the former case, a large Euler buckling force is generated on the MT tip away from the nucleus denoted by $|\vec{f}_{MT-buckle}^{nuc}| = D/l_{MT}^2$, where D is the flexural rigidity of the MT, l_{MT} is the instantaneous MT length, and the resultant buckling force is $\vec{F}_{MT-buckle}^{nuc} = \sum_{MTs} \vec{f}_{MT-buckle}^{nuc}$. In the latter scenario, a large pulling force is generated on the MT tip toward the nucleus as cytoplasmic dyneins (residing on the outer nuclear surface) move toward the negative end of the interacting MT. This force is expressed as $|\vec{f}_{dyn}^{nuc}| = l_{MT}^{nuc} \lambda_{dyn}^{nuc} f_{dyn}^s$, where l_{MT}^{nuc} is the instantaneous sliding length of the MT along the nuclear membrane, λ_{dyn}^{nuc} is the linear density of the cytoplasmic dyneins along the MT track on the nucleus, f_{dyn}^s is the force produced by a single dynein, and therefore the resultant force is $\vec{F}_{dyn}^{nuc} = \sum_{MTs} \vec{f}_{dyn}^{nuc}$.

APPENDIX B: DETAILED DESCRIPTION OF 1D ANALYTICAL MODEL

a. Description of pushing forces

When a microtubule emanates out of the CS and grows all the way to the cell membrane, a steric pushing force will be generated at the MT tip-cell membrane contact that "pushes" the MT tip away from the membrane. However, this instantaneous cortical pushing force originating at the cell membrane ($F_{MT-hit}^{cell-mem}$) will be transmitted via the corresponding MT to the CS. It is evident from the schematic sketch [Fig. 8(a)] of the 1D model that $F_{MT-hit}^{cell-mem}$ pushes the CS away from the cell membrane toward the nucleus.

We consider that the MTs nucleating from the CS exhibit exponential length distribution: $N(l) \propto e^{-l/L_{MT}^{av}}$, where L_{MT}^{av} is the average MT length characterized by its intrinsic dynamic instability parameters [28]. Hence,

$$F_{MT-hit}^{cell-mem} = A e^{-(r_{cell}-x)/L_{MT}^{av}}. \quad (B1)$$

A is the maximal force contribution from $F_{MT-hit}^{cell-mem}$ proportional to the number of MTs that hit the cell membrane
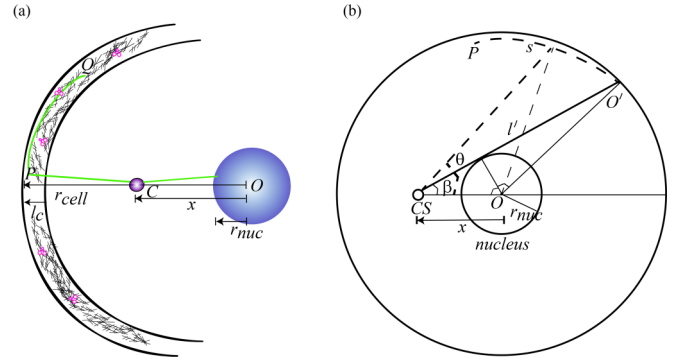

FIG. 8. 1D and 2D mathematical model for CS positioning. (a) In the 1D model, the origin (O) is set at the center of the nucleus (blue sphere) having radius r_{nuc}. The CS is placed at a dynamic position x relative to the origin (O) denoted by C. r_{cell} denotes the radius of the cell. The width of the cortex is taken to be l_c. The green lines represent MTs. PQ is the MT segment undergoing sliding along the cortex. The black mesh within the cortex represents actin arrays. The white-magenta objects represent cortical dynein. (b) In the 2D model, the origin is set at the cell center with the nucleus (radius r_{nuc}) being localized at the origin (O). The CS is positioned at a distance x relative to the origin. θ depicts the angle at which the MT is nucleating out relative to the axis joining the CS and the origin. At $\theta = \beta$ the MT being tangent to the NE hits the cortex if it grows up to a length l'. l' varies with the variation in θ. $O'P$ represents the MT segment (arc s) sliding along the cortex.

segment facing the CS and experience a pushing force of 1 pN per MT.

Similarly, as depicted in the model schematic [Fig. 8(a)] some of the MTs keep elongating and hit the nuclear surface (NE) too. MT tips upon hitting the nuclear surface also experience a pushing force (F_{MT-hit}^{nuc}) which pushes the CS away from the nucleus. It is evident that F_{MT-hit}^{nuc} and $F_{MT-hit}^{cell-mem}$ are oppositely directed. The magnitude of F_{MT-hit}^{nuc} is less than $F_{MT-hit}^{cell-mem}$ because the number of MTs showering onto the nuclear surface is significantly lower than the number of MTs hitting the cell membrane (as $r_{nuc} < r_{cell}$). If we consider that the number of MTs hitting the cell membrane or the nucleus is proportional to the surface area of the cell wall or the nucleus then

$$F_{MT-hit}^{nuc} = A \left(\frac{r_{nuc}}{r_{cell}} \right)^2 e^{-(x-r_{nuc})/L_{MT}^{av}}. \quad (B2)$$

b. Description of pulling forces

When a microtubule nucleates out of the CS and keeps growing until it penetrates into the cortex, it experiences a pulling from the dyneins anchored at the cortex [11,29]. The pulling is proportional to the penetration depth of the MT into the cortex. As depicted in the schematic diagram Fig. 8(a), a growing MT with a nonzero penetration depth into the cortex can also undergo "lateral sliding" along the cortex preceded by a bending within the cortex [segment PQ; Fig. 8(a)]. The total contribution to the cortical pulling (F_{dyn}^{cor}) stems out of the dynein mediated pulling associated with the uncurled segment within the cortex together with the additional contribution from anchored dyneins at the sliding arc of the bent MT segment [segment PQ; Fig. 8(a)].

The contribution from the uncurled MT segment within the cortex $F_{\text{dyn}}^{\text{cor (uncurled)}}$ is

$$
\begin{aligned}
F_{\text{dyn}}^{\text{cor (uncurled)}} &= B\lambda_{\text{dyn}}^{\text{cor}} \int_{r_{\text{cell}}-x-l_c}^{r_{\text{cell}}-x} ds\, e^{-(s-x)/L_{\text{MT}}^{av}} \\
&= B\lambda_{\text{dyn}}^{\text{cor}} L_{\text{MT}}^{av} e^{-(s-x)/L_{\text{MT}}^{av}} \Big|_{r_{\text{cell}}-x}^{r_{\text{cell}}-x-l_c} \\
&= B\lambda_{\text{dyn}}^{\text{cor}} L_{\text{MT}}^{av} (e^{l_c/L_{\text{MT}}^{av}} - 1)\, e^{-(r_{\text{cell}}-2x)/L_{\text{MT}}^{av}}
\end{aligned}
$$
(B3)

and the contribution from the "bent" sliding arc $F_{\text{dyn}}^{\text{cor(sliding arc)}}$ is

$$
\begin{aligned}
F_{\text{dyn}}^{\text{cor(sliding arc)}} &= B\lambda_{\text{dyn}}^{\text{cor}} \int_{0}^{\infty} ds\, e^{-(r_{\text{cell}}-x+s)/L_{\text{MT}}^{av}} \\
&= B\lambda_{\text{dyn}}^{\text{cor}} L_{\text{MT}}^{av} e^{-(r_{\text{cell}}-x+s)/L_{\text{MT}}^{av}} \Big|_{\infty}^{0} \\
&= B\lambda_{\text{dyn}}^{\text{cor}} L_{\text{MT}}^{av} e^{-(r_{\text{cell}}-x)/L_{\text{MT}}^{av}}.
\end{aligned}
$$
(B4)

In the above integral, the lower and upper limits are taken to be 0 and ∞, respectively. Owing to the intrinsic stochastic nature of the MT dynamics, we expect that a distinct subset of the MTs sliding along the cortex will grow significantly long (coursing out a longer sliding arc) and another subset will have MTs which would not elongate that much along the cortex and end up having relatively shorter sliding arcs. While performing the above integral, we estimate the net contribution stemming out of the cumulative sum over all possible arc lengths spanned by the sliding MTs within the cortex. In principle, the referred summation over all possible arc lengths could be much greater than the arc length of the confined geometry (e.g., the cell having radius r_{cell} and perimeter $2\pi r_{\text{cell}}$). Thus the upper limit in the above integral accounting for the summation over all possible arc lengths traced by the MTs sliding along the cortex is taken to be ∞. The above-mentioned argument of considering the upper limit as ∞ in the integral over all possible arc lengths also withholds in the scenario where we calculate the contribution of net pulling force originating from the NE.

Hence the total cortical pulling $F_{\text{dyn}}^{\text{cor}}$ is

$$
F_{\text{dyn}}^{\text{cor}} = F_{\text{dyn}}^{\text{cor (uncurled)}} + F_{\text{dyn}}^{\text{cor(sliding arc)}}.
$$
(B5)

Hence,

$$
\begin{aligned}
F_{\text{dyn}}^{\text{cor}} = B\lambda_{\text{dyn}}^{\text{cor}} L_{\text{MT}}^{av} \big[&(e^{l_c/L_{\text{MT}}^{av}} - 1) e^{-(r_{\text{cell}}-2x)/L_{\text{MT}}^{av}} \\
&+ e^{-(r_{\text{cell}}-x)/L_{\text{MT}}^{av}} \big].
\end{aligned}
$$
(B6)

Here B is also proportional to the average number of MTs hitting the cell cortex.

Similarly, a subset of MTs nucleating out of the CS grows and grazes along the nuclear surface upon reaching NE. The anchored dyneins on the nuclear surface interact with the grazing MT segments and gives rise to a net pulling of the CS toward the nucleus. We can compute the total pulling force $F_{\text{dyn}}^{\text{nuc}}$ as described in the following:

$$
\begin{aligned}
F_{\text{dyn}}^{\text{nuc}} &= \beta\lambda_{\text{dyn}}^{\text{nuc}} \int_{0}^{\infty} ds\, e^{-(x-r_{\text{nuc}}+s)/L_{\text{MT}}^{av}} \\
&= \beta\lambda_{\text{dyn}}^{\text{nuc}} e^{-(x-r_{\text{nuc}})/L_{\text{MT}}^{av}} \int_{0}^{\infty} ds\, e^{-s/L_{\text{MT}}^{av}}
\end{aligned}
$$

$$
\begin{aligned}
&= \beta\lambda_{\text{dyn}}^{\text{nuc}} L_{\text{MT}}^{av} e^{-(x-r_{\text{nuc}})/L_{\text{MT}}^{av}} e^{-s/L_{\text{MT}}^{av}} \Big|_{\infty}^{0} \\
&= \beta\lambda_{\text{dyn}}^{\text{nuc}} L_{\text{MT}}^{av} e^{-(x-r_{\text{nuc}})/L_{\text{MT}}^{av}}.
\end{aligned}
$$
(B7)

Here β is proportional to number of MTs grazing the nuclear surface. β can be approximated to be $B(\frac{r_{\text{nuc}}}{r_{\text{cell}}})^2$. Hence

$$
F_{\text{dyn}}^{\text{nuc}} = B\left(\frac{r_{\text{nuc}}}{r_{\text{cell}}}\right)^2 \lambda_{\text{dyn}}^{\text{nuc}} L_{\text{MT}}^{av} e^{-(x-r_{\text{nuc}})/L_{\text{MT}}^{av}}.
$$
(B8)

c. Description of buckling forces

A dynamic MT within the cortex has a possibility of undergoing buckling. Buckling in the vicinity of the cortex gives rise to a length dependent "pushing" force that increases with the squared inverse length of the MT [5]. MTs grazing the nuclear surface also undergo buckling. According to the model schematic, forces produced due to the cortical buckling and the nuclear buckling are oppositely directed and thus compete with each other during CS positioning. We have taken the following form for the force produced by cortical buckling ($F_{\text{MT-buckle}}^{\text{cell-mem}}$):

$$
F_{\text{MT-buckle}}^{\text{cell-mem}} = \frac{D}{(r_{\text{cell}} - x)^2} e^{-(r_{\text{cell}}-x)/L_{\text{MT}}^{av}}.
$$
(B9)

Similarly for buckling on the nuclear surface $F_{\text{nuc}}^{\text{buckle}}$ is taken as

$$
F_{\text{MT-buckle}}^{\text{nuc}} = \frac{D'}{(x - r_{\text{nuc}})^2} e^{-(x-r_{\text{nuc}})/L_{\text{MT}}^{av}}.
$$
(B10)

D' can be approximated as $D(\frac{r_{\text{nuc}}}{r_{\text{cell}}})^2$ since the number of MTs falling onto a surface is proportional to the area of that surface.

d. Description of steric forces

We have considered steric repulsion between the CS and cell wall and the CS and nucleus. The CS–cell wall steric repulsion $F_{\text{wall}}^{\text{steric}}$ is taken as

$$
F_{\text{cell-mem}}^{\text{steric}} = Ce^{-\zeta(r_{\text{cell}}-x)/L_{\text{MT}}^{av}}.
$$
(B11)

Similarly the CS-nucleus steric repulsion $F_{\text{nuc}}^{\text{steric}}$ is

$$
F_{\text{nuc}}^{\text{steric}} = C'e^{-\zeta'(x-r_{\text{nuc}})/L_{\text{MT}}^{av}}.
$$
(B12)

For simplicity we assume $C = C'$ and $\zeta = \zeta'$. Here C and C' denote the amplitudes of the forces generated due to the steric interactions whereas ζ and ζ' determine the range of the steric forces. The higher the value (positive) of ζ (or ζ'), the more rapidly the magnitude of the force falls off with increase in distance, clearly manifesting the short-range nature of the interaction.

In order to take in to account the finite size of the CS (r_{CS}), in the nuclear force expression r_{nuc} is replaced by $r_{\text{nuc}} \to r_{\text{nuc}} + r_{\text{CS}}$ and in the cortical force expressions r_{cell} is replaced by $r_{\text{cell}} \to r_{\text{cell}} - r_{\text{CS}}$ where r_{CS} is the radius of the CS.

APPENDIX C: DETAILED DESCRIPTION OF 2D ANALYTICAL MODEL

a. Pushing forces

In 2D we can separate out the net instantaneous pushing force contributions into two parts, force transduction from the right cell membrane $F_{MT-hit}^{cell-mem(R)}$, force transduction from the left cell membrane $F_{MT-hit}^{cell-mem(L)}$ accounting for the instantaneous cortical push. Evidently, $F_{MT-hit}^{cell-mem(R)}$ and $F_{MT-hit}^{cell-mem(L)}$ oppose each other. $F_{MT-hit}^{cell-mem(R)}$ has a contribution from the whole of the right cell membrane barring the segment shielded by the nucleus which is acting as a steric obstacle for the MTs reaching the right cell membrane. Hence

$$F_{MT-hit}^{cell-mem(R)} = \tilde{A} n_R \int_{\beta}^{\pi/2} d\theta \cos\theta \, e^{-l'/L_{MT}^{av}}. \tag{C1}$$

Here n_R is the number of MTs on the right side of the CS not obstructed by the nucleus. $\tilde{A}$ is the maximal contribution from the instantaneous cortical push for a single MT. The $\cos\theta$ factor comes into play because we have considered that the microtubules are hitting the cell membrane at a finite angle (θ) [Fig. 8(b)]. Hence, only a component of the force along the X axis is responsible for mobilizing the CS along the X axis. Note that here the representative X axis does not allude to the formal space-fixed X axis in the reference frame. Rather any line joining the CS and the center of the nucleus is represented as the X axis with the origin being set at the center of the nucleus. The intrinsic radial symmetry of the geometric confinement considered here, more precisely the circular cell and the circular nucleus (in 2D) allows us to place the CS at any random location within the cell and map the relative radial distance between the CS and the center of the nucleus as x. In the current analytical 2D model construction, we assume the "immobile" nucleus to be localized at the cell center for the sake of simplicity. Thus the origin of the reference frame under consideration is always placed at the center of the cell. It is evident from the radial symmetry of the default structural template of the 2D mathematical model that only the radial force components acting on the CS survive and radially mobilize the CS along the line joining the CS and the center of the nucleus, namely the X axis with the origin located at the cell center. However, the transverse force components acting perpendicular to the radial axis (X axis denoting the line joining the CS and the origin which is set at the center of the nucleus or cell) nullify each other. Therefore, it is quite reasonable to neglect any movement of the CS along the transverse direction (Y axis) without any loss of generality. The consideration of radial symmetry breaks down if instead of isotropic nucleation of MTs in all directions, MT nucleation is biased in a spatially preferential direction, which is not taken into account in this study.

Now,

$$\vec{l'} + \vec{x} = \vec{r}_{cell}, \tag{C2}$$

$$r_{cell}^2 = l'^2 + x^2 - 2l'x\cos(\theta), \tag{C3}$$

$$l' = \tfrac{1}{2}\left[2x\cos\theta \pm \sqrt{4x^2\cos^2\theta - 4(x^2 - r_{cell}^2)}\right],$$

$$l' = x\cos\theta \pm \sqrt{r_{cell}^2 - x^2\sin^2\theta}. \tag{C4}$$

When $\theta = \pi$, $l' = -x \pm r_{cell} = r_{cell} - x$ (choosing the positive sign). Hence,

$$l' = x\cos\theta + \sqrt{r_{cell}^2 - x^2\sin^2\theta}. \tag{C5}$$

If n_L is the total number of MTs on the left side of the CS, one can establish a relation between n_R and n_L by the following expression,

$$n_R = n_L[1 - (r_{nuc}/r_{cell})^2]. \tag{C6}$$

Evidently $n_L - n_R$ is the number of MTs directed toward the nucleus. Plugging the above expression into Eq. (C1) we obtain

$$F_{MT-hit}^{cell-mem(R)} = \tilde{A} n_R \int_{\beta}^{\pi/2} e^{-l'/L_{MT}^{av}} \cos\theta \, d\theta, \tag{C7}$$

$$e^{-l'/L_{MT}^{av}} = e^{-\frac{1}{L_{MT}^{av}}(x\cos\theta + \sqrt{r_{cell}^2 - x^2\sin^2\theta})}$$

$$= 1 - \frac{1}{L_{MT}^{av}}\left[x\cos\theta + \sqrt{r_{cell}^2 - x^2\sin^2\theta}\right]$$

$$= 1 - \frac{1}{L_{MT}^{av}}\left[x\cos\theta + r_{cell} - \frac{x^2}{2r_{cell}}\sin^2\theta\right]. \tag{C8}$$

Hence,

$$F_{MT-hit}^{cell-mem(R)} = \tilde{A} n_R \int_{\beta}^{\pi/2} \cos\theta \, d\theta$$

$$- \tilde{A} n_R \int_{\beta}^{\pi/2} \frac{1}{L_{MT}^{av}}\left(x\cos^2\theta + r_{cell}\cos\theta\right.$$

$$\left. - \frac{x^2}{2r_{cell}}\sin^2\theta\cos\theta\right)d\theta$$

$$= \tilde{A} n_R \left\{(1 - \sin\beta) - \frac{r_{cell}}{L_{MT}^{av}}(1 - \sin\beta)\right.$$

$$- \frac{x}{2L_{MT}^{av}}\left[(\pi/2 - \beta) - \frac{1}{2}\sin 2\beta\right]$$

$$\left. + \frac{x^2}{6r_{cell}L_{MT}^{av}}(1 - \sin^3\beta)\right\}. \tag{C9}$$

Similarly, the pushing force from the left side of the CS $F_{MT-hit}^{cell-mem(L)}$,

$$F_{MT-hit}^{cell-mem(L)}$$

$$= \tilde{A} n_L \int_{\pi/2}^{\pi} e^{-l'/L_{MT}^{av}} \cos\theta \, d\theta$$

$$= \tilde{A} n_L \left[\sin\theta - \frac{r_{cell}}{L_{MT}^{av}}\sin\theta\right.$$

$$\left. - \frac{x}{2L_{MT}^{av}}\left(\theta + \frac{1}{2}\sin 2\theta\right) + \frac{x^2}{6r_{cell}L_{MT}^{av}}\sin^3\theta\right]_{\pi/2}^{\pi}$$

$$= \tilde{A} n_L \left[\frac{r_{cell}}{L_{MT}^{av}} - 1 - \frac{\pi x}{4L_{MT}^{av}} - \frac{x^2}{6r_{cell}L_{MT}^{av}}\right].$$

b. Pulling forces due to MT sliding at cortex

The pulling force contribution from the right cortex due to MT sliding is

$$
F_{\text{dyn}}^{\text{cor}(R)} = \tilde{B} n_R \lambda_{\text{dyn}}^{\text{cor}} \int_\beta^{\pi/2} \cos\theta \, d\theta \int_0^\infty e^{-(s+l')/L_{\text{MT}}^{av}} ds = \tilde{B} n_R \lambda_{\text{dyn}}^{\text{cor}} L_{\text{MT}}^{av} \int_\beta^{\pi/2} d\theta \cos\theta [e^{-(s+l')/L_{\text{MT}}^{av}}]_\infty^0
$$

$$
= \tilde{B} n_R \lambda_{\text{dyn}}^{\text{cor}} L_{\text{MT}}^{av} \int_\beta^{\pi/2} d\theta \cos\theta \, e^{-l'/L_{\text{MT}}^{av}} = \tilde{B} n_R \lambda_{\text{dyn}}^{\text{cor}} L_{\text{MT}}^{av} \left\{ (1 - \sin\beta) - \frac{r_{\text{cell}}}{L_{\text{MT}}^{av}} (1 - \sin\beta) \right.
$$

$$
\left. - \frac{x}{2 L_{\text{MT}}^{av}} \left[(\pi/2 - \beta) - \frac{1}{2} \sin 2\beta \right] + \frac{x^2}{6 r_{\text{cell}} L_{\text{MT}}^{av}} (1 - \sin^3\beta) \right\}.
$$

Similarly,

$$
F_{\text{dyn}}^{\text{cor}(L)} = \tilde{B} n_L \lambda_{\text{dyn}}^{\text{cor}} \int_{\pi/2}^\pi \cos\theta \, d\theta \int_0^\infty e^{-(s+l')/L_{\text{MT}}^{av}} ds = \tilde{B} n_L \lambda_{\text{dyn}}^{\text{cor}} L_{\text{MT}}^{av} \int_{\pi/2}^\pi d\theta \cos\theta \, e^{-l'/L_{\text{MT}}^{av}}
$$

$$
= \tilde{B} n_L \lambda_{\text{dyn}}^{\text{cor}} L_{\text{MT}}^{av} \left(\frac{r_{\text{cell}}}{L_{\text{MT}}^{av}} - 1 - \frac{\pi x}{4 L_{\text{MT}}^{av}} - \frac{x^2}{6 r_{\text{cell}} L_{\text{MT}}^{av}} \right). \tag{C10}
$$

$\tilde{B}$ is the prefactor determining the strength of dynein pull per MT. For simplicity in pulling force expression, the contribution from the uncurled segment of the MT in the cortex is ignored. This simplification is not going to affect the force balance landscape since it turns out that the "uncurled" contribution in net pulling is very small.

c. Buckling forces

In a fashion similar to the prescription we used in the case of pushing forces, we can also separate the net buckling force contribution on the CS in the following manner: force transduction from the right cell membrane $F_{\text{MT-buckle}}^{\text{cell-mem}(R)}$, force transduction from the left cell membrane $F_{\text{MT-buckle}}^{\text{cell-mem}(L)}$. Force due to the MT buckling transition at the right cell membrane

$$
F_{\text{MT-buckle}}^{\text{cell-mem}(R)} = \tilde{D} n_R \int_\beta^{\pi/2} \frac{e^{-l'/L_{\text{MT}}^{av}}}{l'^2} \cos\theta \, d\theta = \tilde{D} n_R \int_\beta^{\pi/2} \left(\frac{1}{l'^2} - \frac{1}{L_{\text{MT}}^{av} l'} \right) \cos\theta \, d\theta,
$$

$$
l' = x\cos\theta + \sqrt{r_{\text{cell}}^2 - x^2 \sin^2\theta} = x\cos\theta + r_{\text{cell}} \sqrt{1 - \frac{x^2 \sin^2\theta}{r_{\text{cell}}^2}} = r_{\text{cell}} \left(1 - \frac{x^2 \sin^2\theta}{2 r_{\text{cell}}^2} + \frac{x\cos\theta}{r_{\text{cell}}} \right), \tag{C11}
$$

$$
\frac{1}{l'} = \frac{1}{r_{\text{cell}}} \left[1 + \left(\frac{x\cos\theta}{r_{\text{cell}}} - \frac{x^2 \sin^2\theta}{2 r_{\text{cell}}^2} \right) \right]^{-1}, \tag{C12}
$$

$$
= \frac{1}{r_{\text{cell}}} \left(1 - \frac{x\cos\theta}{r_{\text{cell}}} + \frac{x^2 \sin^2\theta}{2 r_{\text{cell}}^2} \right), \tag{C13}
$$

$$
\frac{1}{l'^2} = \frac{1}{r_{\text{cell}}^2} \left[1 + \left(\frac{x}{r_{\text{cell}}} \right)^2 - \frac{2x\cos\theta}{r_{\text{cell}}} \right] \quad \text{(dropping higher order terms).} \tag{C14}
$$

Plugging the above expressions into $F_{\text{MT-buckle}}^{\text{cell-mem}(R)}$ we obtain

$$
F_{\text{MT-buckle}}^{\text{cell-mem}(R)} = \tilde{D} n_R \int_\beta^{\pi/2} \left(\frac{1}{r_{\text{cell}}} \right)^2 \left(\frac{x^2}{r_{\text{cell}}^2} + 1 - \frac{2x\cos\theta}{r_{\text{cell}}} \right) \cos\theta \, d\theta
$$

$$
- \frac{\tilde{D} n_R}{L_{\text{MT}}^{av}} \int_\beta^{\pi/2} \left(\frac{1}{r_{\text{cell}}} \right) \left(\cos\theta - \frac{x\cos^2\theta}{r_{\text{cell}}} + \frac{x^2}{2 r_{\text{cell}}^2} \sin^2\theta \cos\theta \right) d\theta
$$

$$
= \tilde{D} n_R \left(\frac{1}{r_{\text{cell}}} \right)^2 \left[\left(\frac{x}{r_{\text{cell}}} \right)^2 \sin\theta + \sin\theta - \frac{x}{r_{\text{cell}}} \left(\theta + \frac{1}{2} \sin 2\theta \right) \right]_\beta^{\pi/2}
$$

$$
- \frac{\tilde{D} n_R}{L_{\text{MT}}^{av}} \frac{1}{r_{\text{cell}}} \left[\sin\theta - \frac{x}{2 r_{\text{cell}}} \left(\theta + \frac{1}{2} \sin 2\theta \right) + \frac{x^2}{6 r_{\text{cell}}^2} \sin^3\theta \right]_\beta^{\pi/2}
$$

$$
= \frac{\tilde{D} n_R}{r_{\text{cell}}^2} \left[\frac{x^2}{r_{\text{cell}}^2} (1 - \sin\beta) + (1 - \sin\beta) - \frac{x}{r_{\text{cell}}} \left(\frac{\pi}{2} - \beta - \frac{1}{2} \sin 2\beta \right) \right] - \frac{\tilde{D} n_R}{r_{\text{cell}} L_{\text{MT}}^{av}}
$$

$$
\times \left[(1 - \sin\beta) - \frac{x}{2 r_{\text{cell}}} \left(\frac{\pi}{2} - \beta - \frac{1}{2} \sin 2\beta \right) + \frac{x^2}{6 r_{\text{cell}}^2} (1 - \sin^3\beta) \right]. \tag{C15}
$$

And $F_{\text{MT-buckle}}^{\text{cell-mem(L)}}$ is given by

$$F_{\text{MT-buckle}}^{\text{cell-mem(L)}} = \tilde{D} n_L \int_{\pi/2}^{\pi} \left(\frac{1}{r_{\text{cell}}}\right)^2 \left(\frac{x^2}{r_{\text{cell}}^2} + 1 - \frac{2x\cos\theta}{r_{\text{cell}}}\right)\cos\theta \, d\theta$$

$$- \frac{\tilde{D} n_L}{L_{\text{MT}}^{av}} \int_{\pi/2}^{\pi} \left(\frac{1}{r_{\text{cell}}}\right)\left(\cos\theta - \frac{x\cos^2\theta}{r_{\text{cell}}} + \frac{x^2}{2r_{\text{cell}}^2}\sin^2\theta\cos\theta\right) d\theta$$

$$= \tilde{D} n_L \left(\frac{1}{r_{\text{cell}}}\right)^2 \left[-\left(\frac{x}{r_{\text{cell}}}\right)^2 - 1 - \frac{\pi x}{2r_{\text{cell}}}\right] - \frac{\tilde{D} n_L}{r_{\text{cell}} L_{\text{MT}}^{av}}\left(-1 - \frac{\pi x}{2r_{\text{cell}}} - \frac{x^2}{6r_{\text{cell}}^2}\right). \tag{C16}$$

$\tilde{D}$ contains the information of flexural rigidity per MT [5].

d. Forces originating at nucleus

The nuclear force expressions remain the same as in our 1D model if we consider the size of the nucleus to be reasonably smaller than the cell size. In the current parameter regime, only ~5 MTs out of 50 MTs growing on the right side of the CS reach the NE. Hence, the force transduction at the NE is significantly lower than forces acting at the cortical milieu. The significantly smaller size of the nucleus and relatively small magnitude of forces at the NE validate our consideration of 1D force expressions in the quasi-2D model. The pushing force contribution from the NE $F_{\text{MT-hit}}^{\text{nuc}}$ is

$$F_{\text{MT-hit}}^{\text{nuc}} = \tilde{A}(n_L - n_R)e^{-(x - r_{\text{nuc}})/L_{\text{MT}}^{av}}. \tag{C17}$$

The pulling force contribution from the NE $F_{\text{dyn}}^{\text{nuc}}$ is

$$F_{\text{dyn}}^{\text{nuc}} = \tilde{B}(n_L - n_R)\lambda_{\text{dyn}}^{\text{nuc}} L_{\text{MT}}^{av} e^{-(x - r_{\text{nuc}})/L_{\text{MT}}^{av}}. \tag{C18}$$

The force generated due to the MT buckling transition at the NE is given by $F_{\text{MT-buckle}}^{\text{nuc}}$

$$F_{\text{MT-buckle}}^{\text{nuc}} = \tilde{D}(n_L - n_R)\frac{e^{-(x - r_{\text{nuc}})/L_{\text{MT}}^{av}}}{(x - r_{\text{nuc}})^2}. \tag{C19}$$

APPENDIX D: STUDY OF CENTROSOME POSITIONING WITH OFF-CENTERED NUCLEUS

We already discussed the effects of the resultant cortical force, the resultant nuclear force, and the combined force (cortical and nuclear) on the CS positioning when the nucleus is at the cell center [Figs. 2(e), 3(e), and 4(a)]. Here we explore the effects of these forces on the CS positioning when the nucleus is off-centered in the cell. The nucleus is positioned in two different off-central places within the cell and the distributions of the forces are investigated as a function of CS-nucleus distance across the permissible range of the CS position (Fig. 9). The first off-central place is considered somewhat close to the midway between the cell membrane and the cell center [Figs. 9(a), 9(c) and 9(e)] and the second one is considered close to the cell membrane [Figs. 9(b), 9(d) and 9(f)]. As shown in Figs. 9(a) and 9(b), the resultant cortical force on CS ($F_{\text{total}}^{\text{cor}}$) is negative (i.e., $F_{\text{total}}^{\text{cor}}$ is directed toward the NE) throughout the range of the CS position. We already noticed that as long as the nucleus is at the cell center, $F_{\text{total}}^{\text{cor}}$ is directed toward the NE throughout the range of CS position [Fig. 2(e)]. Therefore, for any arbitrary position of the nucleus, the resultant cortical force on the CS always pushes it to fall on the NE.

Figures 9(c) and 9(d) show that when the CS is close to the NE, the resultant nuclear force on the CS ($F_{\text{total}}^{\text{nuc}}$) is positive, i.e., directed away from the NE; as the CS-nucleus distance increases, $F_{\text{total}}^{\text{nuc}}$ falls exponentially to zero. We already noticed a similar characteristic of $F_{\text{total}}^{\text{nuc}}$ when the nucleus is positioned at the cell center [Fig. 3(e)]. Thus, the resultant nucleus driven force on the CS always repels it away from the nucleus.

The resultant cortical and nuclear forces ($F_{\text{total}}^{\text{cor \& nuc}}$) acting together on the CS lead to a null force region ~1–2 μm away from the NE [Figs. 9(e) and 9(f)]. If the CS is located closer to the nucleus, the resultant force on the CS is positive and directed away from the NE; on the contrary, when the CS is located slightly farther from the null force region, the resultant force on the CS is negative, i.e., directed toward the NE. Note that the results are qualitatively similar as described in Fig. 4(a), where the nucleus was considered at the cell center. Therefore, we conclude that for any arbitrary position of the nucleus, the combined force (cortical and nuclear) always draws the CS to the perinuclear region. The analytical prescription corroborates the simulation results for the off-centered position of the nucleus.

APPENDIX E: FORCE BALANCE LANDSCAPE IN THE PRESENCE OF SHORTER MTs

We have considered two scenarios for shorter MTs: (1) moderately short MTs (characterized by $L_{\text{MT}}^{av} = 10.0$ μm), (2) severely short MTs (characterized by $L_{\text{MT}}^{av} = 3.0$ μm). For these short MT lengths, here we explore the force balance landscape of CS positioning with our analytic propositions [Figs. 10(a)–10(f)] and the simulation outcomes [Figs. 11(a)–11(f)].

a. Cortical push and pull

For short, fragmented MTs, cortical push dominates over cortical pull for $\lambda_{\text{dyn}}^{\text{cor}} \leqslant 0.2$ μm^{-1} ($L_{\text{MT}}^{av} \sim 3.0$ μm) and $\lambda_{\text{dyn}}^{\text{cor}} \leqslant 0.1$ μm^{-1} ($L_{\text{MT}}^{av} \sim 10.0$ μm) [Fig. 10(a)]. Since $F_{\text{dyn}}^{\text{cor}}$ is proportional to L_{MT}^{av}, for shorter MTs, higher dynein activity [$\lambda_{\text{dyn}}^{\text{cor}}$ one order of magnitude higher than Fig. 5(a)] is required to pave the way for the changeover in CS positioning from NE to cell membrane. While undergoing the spatial changeover, the CS voyages through a region 0.09 μm^{-1} $\leqslant$ $\lambda_{\text{dyn}}^{\text{cor}} \leqslant 0.2$ μm^{-1} for $L_{\text{MT}}^{av} = 3.0$ μm, 0.087 μm^{-1} $\leqslant \lambda_{\text{dyn}}^{\text{cor}} \leqslant$ 0.093 μm^{-1} for $L_{\text{MT}}^{av} = 10.0$ μm [Fig. 10(a) and inset, respectively] having two stable fixed points at NE and cell
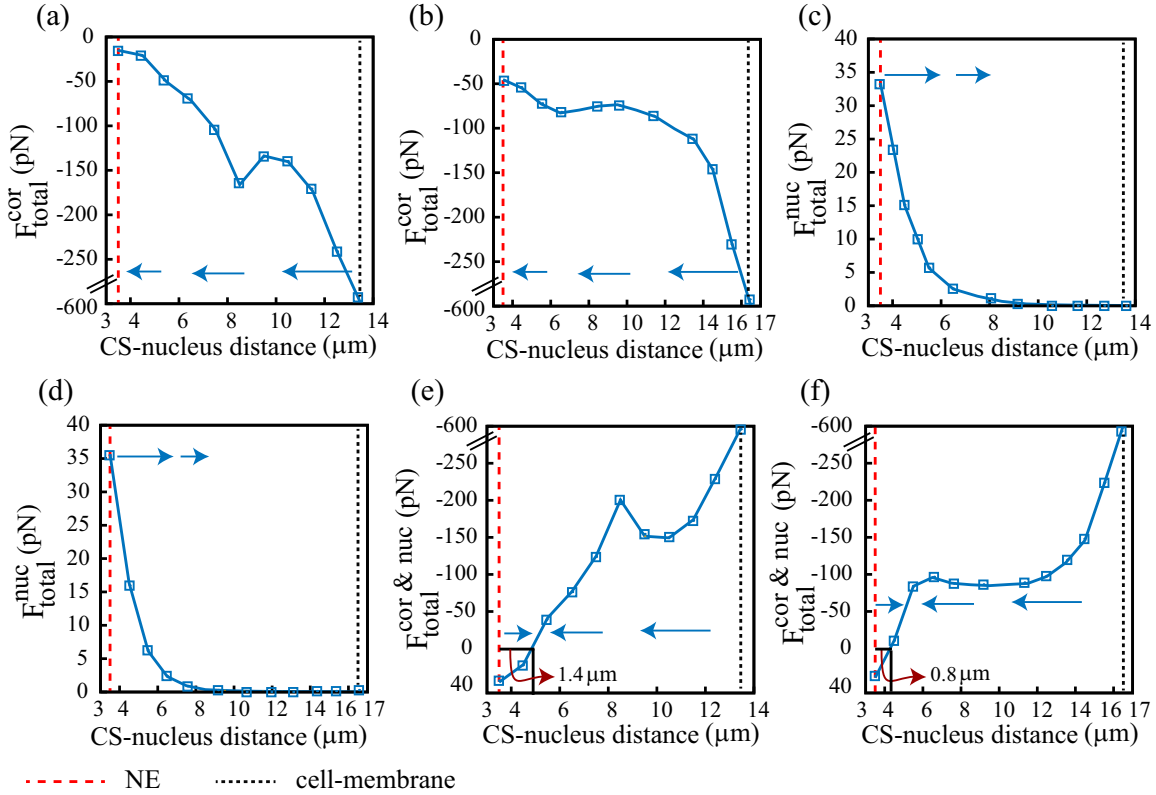
FIG. 9. CS positioning is investigated for off-centered nucleus in the cell. Here we consider two off-central positions of the nucleus: one between the cell membrane and the cell center [(a), (c), and (e)] and the other is close to the cell membrane [(b), (d), and (f)]. (a) and (b) The resultant cortical force on CS ($F_{\text{total}}^{\text{cor}}$) is directed (leftward arrows) toward the NE throughout the range of the CS position. (c) and (d) As the CS moves closer to the NE, the resultant nuclear force ($F_{\text{total}}^{\text{nuc}}$) pushes it away from the NE (rightward arrows). (e) and (f) Due to the combined effort of the resultant cortical force and the resultant nuclear force ($F_{\text{total}}^{\text{cor \& nuc}}$), the CS achieves a stable fixed point, i.e., a zero force region (marked accordingly) at the perinuclear region, i.e., $\sim$1–2 μm away from the NE. If the CS is located on the left of the stable fixed point, $F_{\text{total}}^{\text{cor \& nuc}}$ pushes the CS away from the NE (rightward arrows), whereas if the CS is on the right of the stable fixed point, $F_{\text{total}}^{\text{cor \& nuc}}$ pushes the CS toward the NE (leftward arrows).

membrane, respectively, and another unstable fixed point sandwiched in between. The respective simulation outcome is given in Fig. 11(a). Here it is noticed that with the increase of cortical dynein density, a changeover happens in CS positioning from NE to cell membrane via no string of unstable fixed points for both the L_{MT}^{av} values.

b. Cortical push, pull, and buckle

For short, fragmented MTs, stable fixed points are positioned on the NE as instantaneous push coupled with MT buckling at the cortex wins over the cortical pull for $\lambda_{\text{dyn}}^{\text{cor}} \leqslant$ 1.4 μm^{-1} ($L_{\text{MT}}^{av} \sim 3.0$ μm) and $\lambda_{\text{dyn}}^{\text{cor}} \leqslant 0.5$ μm^{-1} ($L_{\text{MT}}^{av} \sim$ 10.0 μm) [Fig. 10(b)]. Unlike the Fig. 10(a), while undergoing the spatial changeover, the loci of the stable fixed points spans a region in the distance-$\lambda_{\text{dyn}}^{\text{cor}}$ plane ("distance" is CS-nucleus distance) having no unstable fixed point anywhere [Fig. 10(b)]. The respective simulation outcome is given in Fig. 11(b). Here also, it is noticed that with the increase of cortical dynein density, the stable fixed point (for the CS) is shifted toward the cell membrane via no string of unstable fixed points for both the L_{MT}^{av} values.

c. Nuclear push and pull

In the absence of the cortical forces, at lower values of $\lambda_{\text{dyn}}^{\text{nuc}}$, the CS has stable fixed points at the cell membrane owing to the greater contribution of nuclear push ($F_{\text{MT-hit}}^{\text{nuc}}$). As $F_{\text{MT-hit}}^{\text{nuc}}(x)$ and $F_{\text{dyn}}^{\text{nuc}}(x)$ are opposite in sign, the vectorial addition of these two terms is marked by a "zero line" crossover at certain values of x upon stepwise increase in $\lambda_{\text{dyn}}^{\text{nuc}}$. This crossover in the region 3.5 μm $\leqslant$ distance $\leqslant 9.5$ μm is characterized by a sharp spatial transition in CS positioning in the distance-$\lambda_{\text{dyn}}^{\text{nuc}}$ plane [Fig. 10(c)]. Evidently, the smaller the L_{MT}^{av} the higher the dynein density required for the transition. The respective simulation outcome [Fig. 11(c)] runs parallel with this analytic proposition in a qualitative manner.

d. Nuclear push, pull, and buckle

In the case of shorter MTs in the absence of cortical forces the interplay among nuclear push, buckle, and nuclear pull gives rise to a landscape with single stable fixed points for the explored values of $\lambda_{\text{dyn}}^{\text{nuc}}$ (0.0 μm$^{-1} \leqslant \lambda_{\text{dyn}}^{\text{nuc}} \leqslant 10.0$ μm^{-1}). The stable fixed points in the proximity of the NE are $\sim$1.5 μm away from the NE owing to the short-range push originating from the MT buckling at the NE [Fig. 10(d)]. In
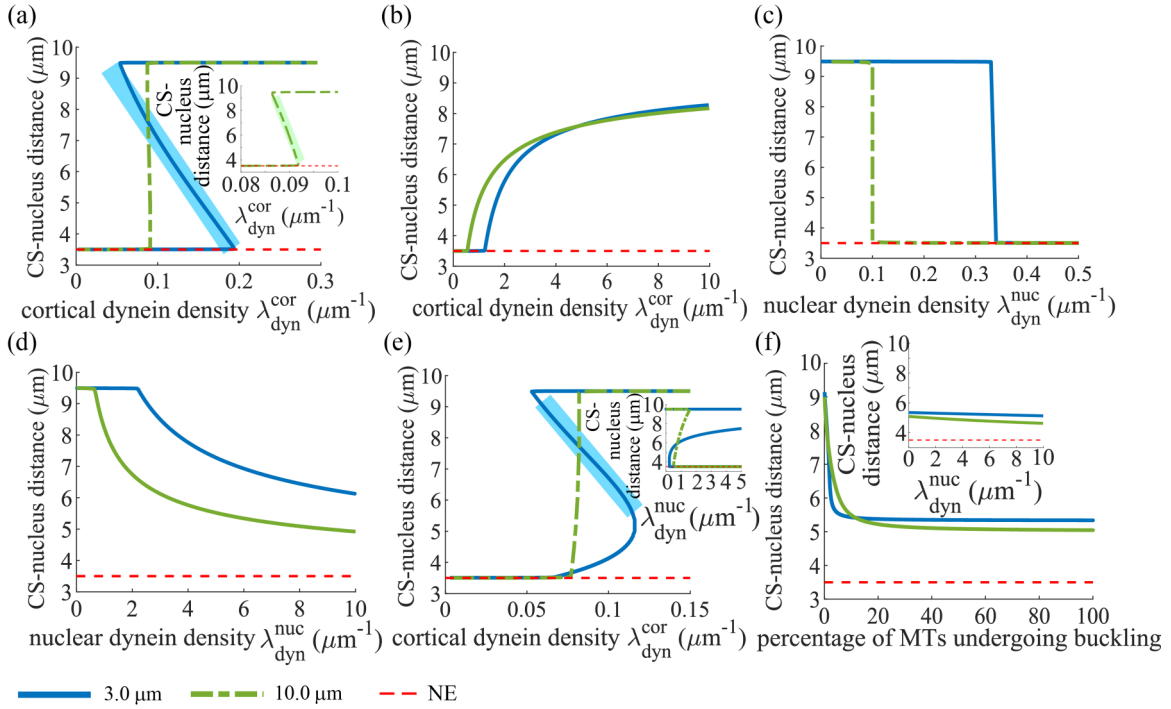
FIG. 10. Short fragmented MTs alter the force balance landscape required for proper CS positioning evincing a change in activity for a myriad of key cortical and nuclear determinants (analytic description in 1D). For all the following figures, the y labels at $3.5\,\mu m$ and $9.5\,\mu m$ mark the position of NE and cell membrane, respectively. (a) Variation in cortical dynein density ($\lambda_{\rm dyn}^{\rm cor}$) triggers a spatial changeover in CS positioning in the presence of instantaneous cortical push and cortical pull. Inset: Loci of stable fixed points with unstable fixed points sandwiched in between for $L_{\rm MT}^{av} = 10.0\,\mu m$. (b) In the presence of MT buckling transition at cell membrane along with cortical push and cortical pull the CS stabilizes $\sim 1.5\,\mu m$ away from the cell membrane at a higher dynein density ($\lambda_{\rm dyn}^{\rm cor} \geqslant 8.0\,\mu m^{-1}$). (c) Variation in nuclear dynein density ($\lambda_{\rm dyn}^{\rm nuc}$) triggers a "sharp" spatial changeover in CS positioning in the presence of instantaneous nuclear push and nuclear pull. (d) In the presence of MT buckling transition at NE along with instantaneous nuclear push and nuclear pull, the CS stabilizes $\sim 0.5\,\mu m$ away from the NE at a higher dynein density ($\lambda_{\rm dyn}^{\rm nuc} \geqslant 0.5\,\mu m^{-1}$ for $L_{\rm MT}^{av} = 10.0\,\mu m$; $\lambda_{\rm dyn}^{\rm nuc} \geqslant 1.0\,\mu m^{-1}$ for $L_{\rm MT}^{av} = 3.0\,\mu m$). (e) Loci of stable and unstable fixed points upon the variation of cortical dynein density when instantaneous cortical push, pull, and nuclear push act in tandem. Inset: Variation in nuclear pull ($\lambda_{\rm dyn}^{\rm nuc}$) leads to a slew of unstable fixed points when cortical push, cortical pull ($\lambda_{\rm dyn}^{\rm cor} = 0.15\,\mu m^{-1}$), and nuclear push act in tandem. (f) Variation in the percentage of MTs undergoing buckling at cell membrane and NE invokes significant distance dependence (CS-nucleus) in the loci of fixed points for the CS in the presence of instantaneous cortical push, cortical pull ($\lambda_{\rm dyn}^{\rm cor} = 0.15\,\mu m^{-1}$) in tandem with instantaneous nuclear push. Inset: Variation in nuclear pull ($\lambda_{\rm dyn}^{\rm nuc}$) in the presence of cortical push, pull ($\lambda_{\rm dyn}^{\rm cor} = 0.15\,\mu m^{-1}$), and buckle (50%) in tandem with nuclear push and buckle (50%) does not alter the CS localization significantly. For $L_{\rm MT}^{av} = 3.0\,\mu m$ a string of unstable fixed points are observed.

the respective simulation outcome [Fig. 11(d)], we observe that despite a huge increase in $\lambda_{\rm dyn}^{\rm nuc}$, the very high nuclear buckling force strongly prevents the CS from coming close to the nucleus.

e. Cortical push and pull in harness with nuclear push and pull

In the absence of nuclear pull, for $L_{\rm MT}^{av} = 10\,\mu m$ the CS position makes a sudden changeover from the NE to the cell membrane upon stepwise increase in $\lambda_{\rm dyn}^{\rm cor}$. For $L_{\rm MT}^{av} = 3.0\,\mu m$ this spatial changeover is gradual and marked by an array of unstable fixed points between the NE and the cell membrane [Fig. 10(e)]. Now at $\lambda_{\rm dyn}^{\rm cor} = 0.15\,\mu m^{-1}$, if $\lambda_{\rm dyn}^{\rm nuc}$ is gradually increased [Fig. 10(e), inset], we obtain a landscape designated by three fixed points, one unstable fixed point sandwiched between two stable points at the NE and cell membrane.

In the respective simulation outcome [Fig. 11(e)], it is noticed that when the nuclear pull is absent and the CS is

driven by cortical push, pull, and nuclear push, the stable fixed point (for the CS) is completely shifted to the cell membrane for the higher values of cortical dynein density ($\lambda_{\rm dyn}^{\rm cor} \geqslant 0.4\,\mu m^{-1}$). Like the analytic proposition, we notice that if the nuclear pull is switched on in this case [Fig. 11(e), inset], a changeover happens in CS positioning from the cell membrane to the NE via a string of unstable fixed points for both the $L_{\rm MT}^{av}$ values.

f. Cortical push, pull, and buckle in harness with nuclear push, pull, and buckle

Evidently in the presence of the cortical push, pull, and buckle in harness with nuclear push and buckle, for $L_{\rm MT}^{av} = 10\,\mu m$ and $L_{\rm MT}^{av} = 3\,\mu m$, the scenario [Fig. 10(f)] closely replicates Fig. 5(e). The respective simulation outcome in 3D [Fig. 11(f)] shows that for both the $L_{\rm MT}^{av}$ values, the stable fixed point (for the CS) does not shift its position considerably with the alteration of the MT buckling chance at the NE and at the
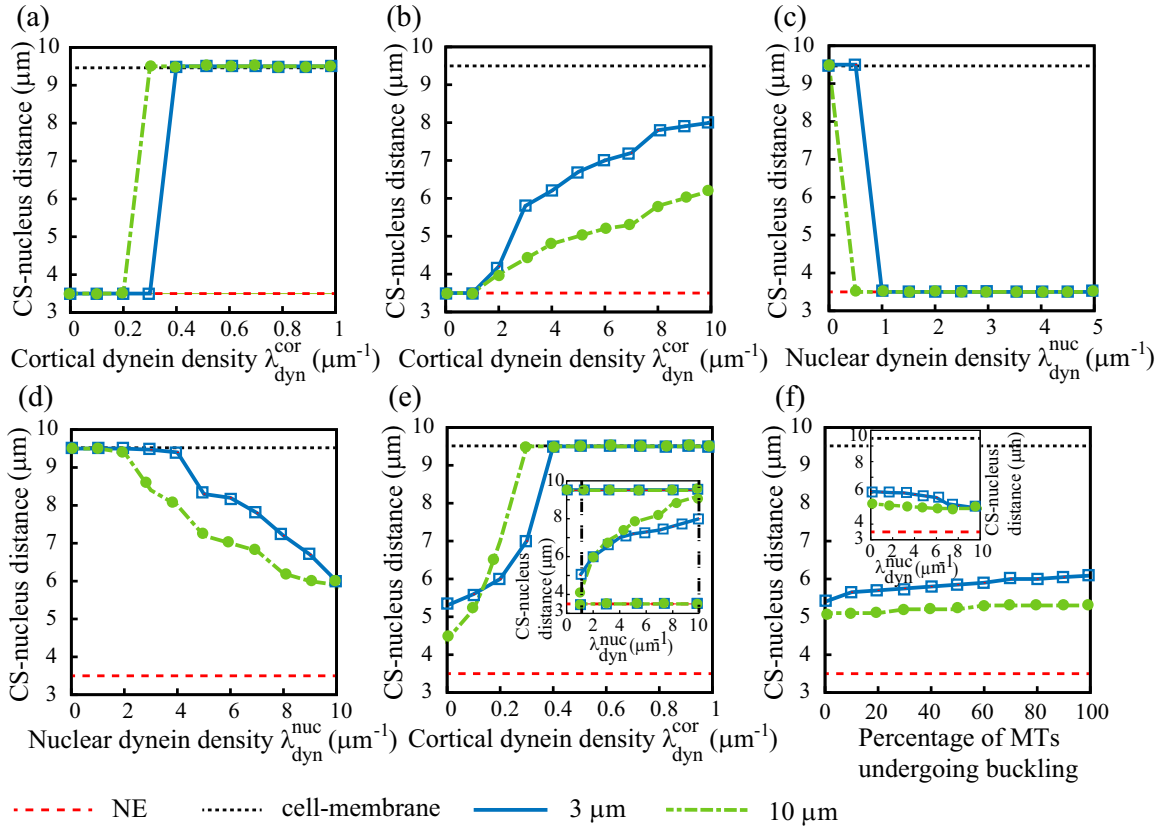
FIG. 11. Short MTs alter the force balance landscape required for proper CS positioning evincing a change in activity for a myriad of key cortical and nuclear determinants. Average MT lengths are 3 μm (solid blue) and 10 μm (dashed green). (a) Variation in cortical dynein density (λ_{dyn}^{cor}) triggers a spatial changeover in CS positioning in the presence of instantaneous cortical push and cortical pull. (b) In the presence of MT buckling transition at cell membrane along with cortical push and cortical pull the CS stabilizes ~1.5 μm (3.5 μm) away from the cell membrane at a very high dynein density ($\lambda_{dyn}^{cor} = 10$ μm^{-1}) for $L_{MT}^{av} = 3$ μm ($L_{MT}^{av} = 10$ μm). (c) Variation in nuclear dynein density (λ_{dyn}^{nuc}) triggers a "sharp" spatial changeover in CS positioning in the presence of instantaneous nuclear push and pull. (d) In the presence of MT buckling at the NE along with instantaneous nuclear push and pull, the CS stabilizes ~2.5 μm away from the NE at a very high dynein density ($\lambda_{dyn}^{nuc} = 10$ μm^{-1}) for $L_{MT}^{av} = 10$ μm and $L_{MT}^{av} = 3$ μm. (e) Locus of stable fixed points as a function of the cortical dynein density when instantaneous cortical push, pull, and nuclear push act in tandem. Inset: Variation in nuclear pull (λ_{dyn}^{nuc}) leads to a slew of unstable fixed points when cortical push, cortical pull ($\lambda_{dyn}^{nuc} = 0.03$ μm^{-1}), and nuclear push act in tandem. (f) For both L_{MT}^{av}, variation in the percentage of MTs undergoing buckling at cell membrane and NE does not invoke significant distance dependence (CS-nucleus) in the locus of the stable fixed points for the CS. Here CS is subjected to the instantaneous cortical push, pull ($\lambda_{dyn}^{cor} = 0.03$ μm^{-1}) in tandem with nuclear push. Inset: Variation in the nuclear pull (λ_{dyn}^{nuc}) in the presence of cortical push, pull ($\lambda_{dyn}^{cor} = 0.03$ μm^{-1}), and buckle (50%) in tandem with nuclear push and buckle (50%) does not alter the CS localization significantly.

cell membrane. Interestingly, this scenario closely replicates Fig. 6(d). The dissimilarity appears between the theoretical outcome (1D) and the simulation outcome (3D) because of dimensional difference.

[1] A. V. Burakov and E. S. Nadezhdina, Cell Biol. Int. **37**, 95 (2013).

[2] J. F. Aronson, J. Cell Biol. **51**, 579 (1971).

[3] J. B. Manneville and S. Etienne-Manneville, Biol. Cell **98**, 557 (2006).

[4] J. Zhu, A. Burakov, V. Rodionov, and A. Mogilner, Mol. Biol. Cell **21**, 4418 (2010).

[5] G. Letort, F. Nedelec, L. Blanchoin, and M. Thery, Mol. Biol. Cell **27**, 2833 (2016).

[6] A. Burakov, E. Nadezhdina, B. Slepchenko, and V. Rodionov, J. Cell Biol. **162**, 963 (2003).

[7] I. B. Brodsky, A. V. Burakov, and E. S. Nadezhdina, Cell Motil. Cytoskeleton **64**, 407 (2007).

[8] K. Kimura and A. Kimura, BioArchitecture **1**, 74 (2011).

[9] I. V. Maly, Commun. Integr. Biol. **4**, 230 (2011).

[10] M. Vleugel, M. Kok, and M. Dogterom, Cell Adhes. Migr. **10**, 475 (2016).

[11] J. Howard and C. Garzon-Coral, BioEssays **39**, 1700122 (2017).

[12] T. E. Holy, M. Dogterom, B. Yurke, and S. Leibler, Proc. Natl. Acad. Sci. U.S.A. **94**, 6228 (1997).

[13] M. Ueda, R. Gräf, H. K. MacWilliams, M. Schliwa, and U. Euteneuer, Proc. Natl. Acad. Sci. U.S.A. **94**, 9674 (1997).

[14] N. Tang and W. F. Marshall, J. Cell Sci. **125**, 4951 (2012).

[15] N. Shekhar, J. Wu, R. B. Dickinson, and T. P. Lele, Cell. Mol. Bioeng. **6**, 74 (2013).

[16] J. Elric and S. Etienne-Manneville, Exp. Cell Res. **328**, 240 (2014).

[17] C. P. Brangwynne, F. C. MacKintosh, and D. A. Weitz, Proc. Natl. Acad. Sci. U.S.A. **104**, 16128 (2007).

[18] A. R. Barker, K. V. McIntosh, and H. R. Dawe, Protoplasma **253**, 1007 (2016).

[19] J. Beaudouin, D. Gerlich, N. Daigle, R. Eils, and J. Ellenberg, Cell **108**, 83 (2002).

[20] T. Zhao, O. S. Graham, A. Raposo, and D. St Johnston, Science **336**, 999 (2012).

[21] A. De Simone, A. Spahr, C. Busso, and P. Gönczy, Nat. Commun. **9**, 938 (2018).

[22] P. T. Tran, L. Marsh, V. Doye, S. Inoué, and F. Chang, J. Cell Biol. **153**, 397 (2001).

[23] S. Sutradhar, V. Yadav, S. Sridhar, L. Sreekumar, D. Bhattacharyya, S. K. Ghosh, R. Paul, and K. Sanyal, Mol. Biol. Cell **26**, 3954 (2015).

[24] F. J. McNally, J. Cell Biol. **200**, 131 (2013).

[25] S. Kotak and P. Gönczy, Curr. Opin. Cell Biol. **25**, 741 (2013).

[26] M. Kikumoto, M. Kurachi, V. Tosa, and H. Tashiro, Biophys. J. **90**, 1687 (2006).

[27] M. Soheilypour, M. Peyro, S. J. Peter, and M. R. K. Mofrad, Biophys. J. **108**, 1718 (2015).

[28] N. Ferenz, R. Paul, C. Fagerstrom, A. Mogilner, and P. Wadsworth, Curr. Biol. **19**, 1833 (2009).

[29] J. Howard, Phys. Biol. **3**, 54 (2006).

[30] D. Splinter, M. E. Tanenbaum, A. Lindqvist, D. Jaarsma, A. Flotho, K. L. Yu, I. Grigoriev, D. Engelsma, E. D. Haasdijk, N. Keijzer, J. Demmers, M. Fornerod, F. Melchior, C. C. Hoogenraad, R. H. Medema, and A. Akhmanova, PLoS Biol. **8**, e1000350 (2010).

[31] S. Bolhy, I. Bouhlel, E. Dultz, T. Nayak, M. Zuccolo, X. Gatti, R. Vallee, J. Ellenberg, and V. Doye, J. Cell Biol. **192**, 855 (2011).

[32] O. Azarenko, T. Okouneva, K. W. Singletary, M. Jordan, and L. Wilson, Carcinogenesis **29**, 2360 (2008).

[33] N. M. Rusan, C. J. Fagerstrom, A.-M. C. Yvon, and P. Wadsworth, Mol. Biol. Cell **12**, 971 (2001).

[34] M. Gopalakrishnan and B. S. Govindan, Bull. Math. Biol. **73**, 2483 (2011).

[35] F. Gittes, B. Mickey, J. Nettleton, and J. Howard, J. Cell Biol. **120**, 923 (1993).

[36] B. Alberts, A. Johnson, J. Lewis, M. Raff, K. Roberts, and P. Walter, *Molecular Biology of the Cell*, 4th ed. (Garland Science, New York, 2002), pp. 191–234.

[37] M. Thery, D. Inoue, D. Obino, F. Farina, J. Gaillard, C. Guérin, L. Blanchoin, and A. M. Lennon-Duménil, bioRxiv, doi:10.1101/302190.

[38] N. Fakhri, A. D. Wessel, C. Willms, M. Pasquali, D. R. Klopfenstein, F. C. MacKintosh, and C. F. Schmidt, Science **344**, 1031 (2014).

[39] S. L. Gupton, W. C. Salmon, and C. M. Waterman-Storer, Curr. Biol. **12**, 1891 (2002).

[40] F. Farina, J. Gaillard, C. Guérin, Y. Coute, J. Sillibourne, L. Blanchoin, and M. Théry, Nat. Cell Biol. **18**, 65 (2016).

[41] D. Obino, F. Farina, O. Malbec, P. J. Sáez, M. Maurin, J. Gaillard, F. Dingli, D. Loew, A. Gautreau, M. I. Yuseff, L. Blanchoin, M. Théry, and A. M. Lennon-Duménil, Nat. Commun. **7**, 10969 (2016).

[42] R. Hulspas, A. B. Houtsmuller, J. G. J. Baumann, and N. Nanninga, Exp. Cell Res. **215**, 28 (1994).

[43] C. J. Malone, W. L. Misner, N. L. Bot, M.-C. Tsai, J. M. Campbell, J. Ahringer, and J. G. White, Cell **115**, 825 (2003).

[44] P. Gönczy, Curr. Biol. **14**, R268 (2004).

[45] J. Schmoranzer, J. P. Fawcett, M. Segura, S. Tan, R. B. Vallee, T. Pawson, and G. G. Gundersen, Curr. Biol. **19**, 1065 (2009).

[46] A. Bellion, J.-P. Baudoin, C. Alvarez, M. Bornens, and C. Métin, J. Neurosci. **25**, 5691 (2005).

[47] F. G. Agircan, E. Schiebel, and B. R. Mardin, Philos. Trans. R. Soc. London B **369**, 20130461 (2014).

[48] D. Salina, K. Bodoor, D. M. Eckley, T. A. Schroer, J. B. Rattner, and B. Burke, Cell **108**, 97 (2002).

[49] R. A. Longoria and G. T. Shubeita, PLoS ONE **8**, e67710 (2013).